GENERAL ATOMIC

DIVISION OF GENERAL DYNAMICS

GA-2471

DEVELOPMENT OF MULTIPLYING ASSEMBLY

FINAL REPORT

Contract AT(04-3)-167
Project Agreement No. 7

U. S. Atomic Energy Commission

June 30, 1961

DISCLAIMER

GENERAL ATOMIC

DIVISION OF

GENERAL DYNAMICS

JOHN JAY HOPKINS LABORATORY FOR PURE AND APPLIED SCIENCE

P.O. BOX 608. SAN DIEGO 12. CALIFORNIA

GA-2471

DEVELOPMENT OF MULTIPLYING ASSEMBLY

FINAL REPORT

Contract AT(04-3)-167
Project Agreement No. 7

U. S. Atomic Energy Commission

Work done by:

J. C. Young
J. R. Beyster
P. R. Heid
D. H. Houston
G. D. Trimble

Report written by:

J. C. Young
J. R. Beyster
P. R. Heid
D. H. Houston
G. D. Trimble

Project 95

June 30, 1961

ABSTRACT

A water-moderated multiplying assembly has been designed, constructed, and pulsed with a high-intensity neutron source produced by an electron linear accelerator. Neutron die-away measurements made during the loading operations were correlated with the reactivity of the bare assembly. Neutron-spectra measurements were performed at the final loading.

CONTENTS

Figures

I. INTRODUCTION

This is the final report under Project Agreement No. 7 of Contract AT(04-3)-167 with the U.S. Atomic Energy Commission. The report covers the period from the start of work on May 15, 1960, through June 30, 1961. It describes the design and fabrication of a multiplying assembly, performed under Project Agreement No. 7, and also describes the measurements of neutron spectra and decay constants in the finished assembly, which were subsequently performed under Project Agreement No. 2 of Contract AT(04-3)-167.

The multiplying assembly has been especially tailored to facilitate neutron-spectrum measurements. The motivations for constructing the assembly for this purpose were many. Reactor spectra had never been measured in a water-moderated multiplying assembly despite the importance of these spectra in reactor parameter studies. The pulsed method[1] of measuring spectra is new and has never been adapted for use with multiplying systems. This method allows a direct comparison in some cases between spectra measured in nonmultiplying systems and spectra measured in what is essentially a reactor, thereby ensuring that no significant considerations have been overlooked in the theoretical procedures.

The studies of spectra in nonmultiplying systems performed under the basic contract (Project Agreement No. 2) had, of course, a direct bearing on situations considered here. For example, all spectra measured in water, no matter what the poisoning agent or its concentration, tend to disagree in certain characteristic ways with theoretical predictions. The energy spectrum of the scalar flux disagrees considerably in some energy regions, while the disagreement may be small in other situations. The reason for this discrepancy is not understood, but a possible source of

trouble experimentally is in the spatial distribution of the neutrons in a nonmultiplying system. This distribution is far from the fundamental mode, and residual effects in the spectrum due to spatial effects could be significant. Thus, by measuring the spectrum in a system with the flux more nearly in a fundamental mode, as in the multiplying medium, one can study the importance of this effect. In a sense, the multiplying system gives a closer approximation to infinite-medium conditions for spectral studies. Early in the program of integral neutron thermalization, it became apparent that one could not simulate with moderators and nonmultiplying absorbers all important reactor geometries which require experimental investigation. The use of the multiplying assembly to extend the thermalization studies to actual reactor operating conditions has proven productive.

The program was planned in such a way that, initially, infinite-media or one-dimensional problems could be studied experimentally. For a more complete and useful program, the calculations and design of the subcritical assembly were made so as to make possible the option of taking the assembly to critical. This capability will allow an experimental determination of the critical mass and a complete correlation of the constants used in the reactor calculations with the spectral and decay-constant measurements which were made in the subcritical assembly. The assembly was also designed to permit theory and experiment to be compared in multiplying lattices where pronounced spatial dependence of the neutron spectra exists. This will permit extension of the neutron-thermalization program to many of the problems of spatially-dependent neutron spectra.

Detailed design of the assembly is discussed in Section II, the theory for analysis of data in Section III, reactivity and shielding calculation previous to loading the subcritical assembly in Section IV, experimental investigations and results in Section V, and a summary of results and conclusions in Section VI.

II. DESIGN OF THE ASSEMBLY

The subcritical assembly was designed to approximate as closely as possible a homogeneous one-dimensional bare multiplying assembly. The boundary conditions necessary for the initial experimental program are as follows:

1. At the location for the spectral measurements, local buckling should be such that $\Sigma_a \geq 20\ DB^2$, where Σ_a is the macroscopic absorption cross section, D the diffusion coefficient, and B^2 the geometrical buckling.
2. Neutron generation time or die-away time should not exceed 400 μsec.
3. Neutron multiplication, M, should be such that $20 > M > 4$.
4. Flux depression and self-absorption due to the uranium foils should be small and foils should be close together.
5. Foil assemblies should be rigid, so that water channels do not vary appreciably in thickness.
6. The absorption per hydrogen atom should be ≥ 1 barn.

The boundary conditions were satisfied in the following way at the final loading. Σ_a was calculated to be 0.129 cm^{-1} with $\overline{DB}^2$ equal to 0.0039. The local buckling was determined from flux measurements. For condition 2, the die-away time was measured to be about 409 μsec. The multiplication was measured to be about 10. To satisfy condition 4, the uranium–aluminum plates were spaced 0.125 in. apart and their self-absorption was calculated to be about 5%. Design of the core ensured condition 5. The absorption per hydrogen atom was calculated to be about 2.4 barns/hydrogen atom.

An over-all picture of the subcritical assembly is shown in Fig. 1. The major components of the subcritical assembly include the core tank,

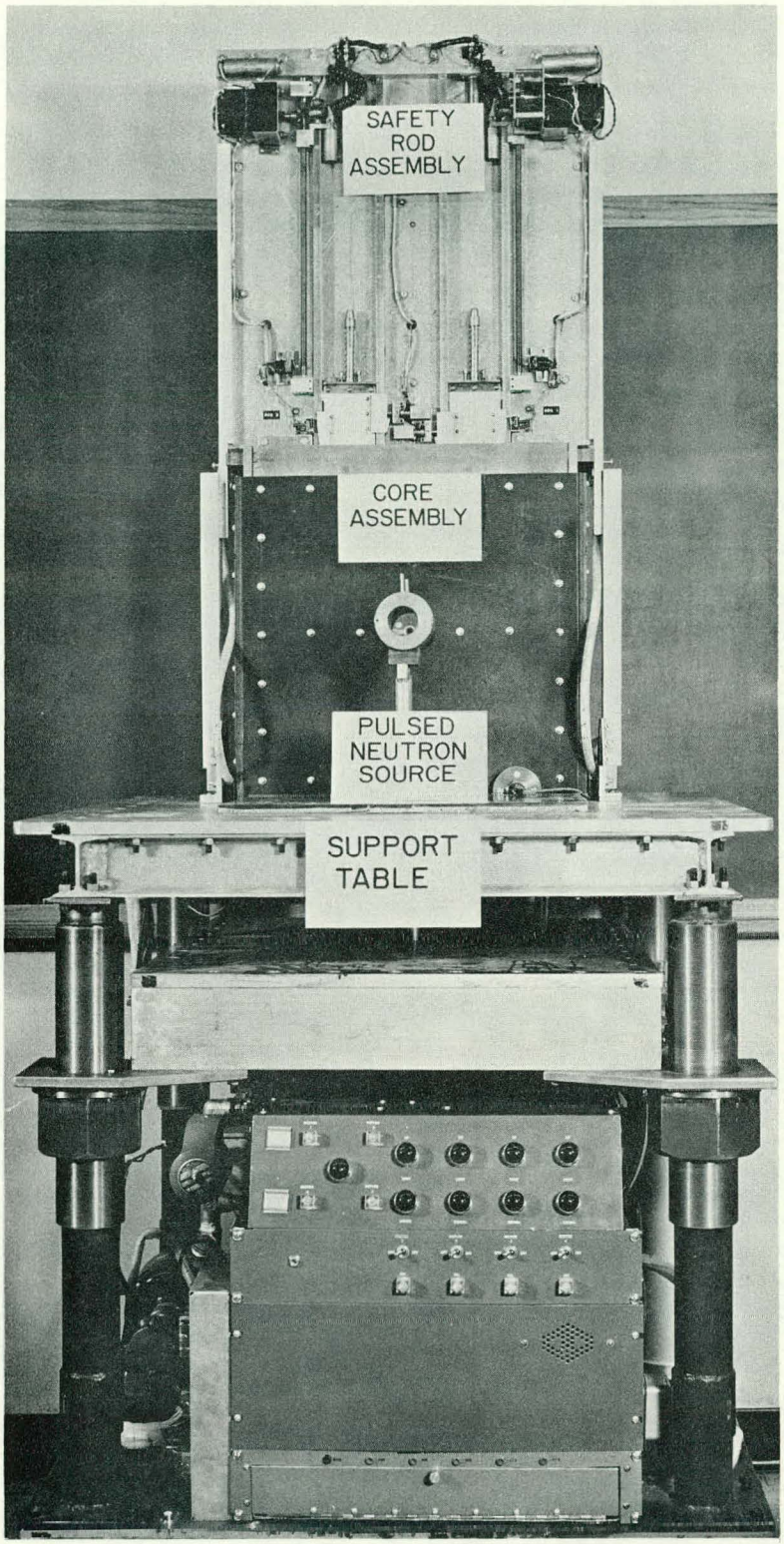

Fig. 1--Configuration of the completed subcritical assembly

fuel plates, support table, safety-rod assembly, and instrumentation.

2.1. CORE TANK

A top view of the core tank and safety-rod assembly is shown in Fig. 2. The tank is a parallelepiped with inside dimensions of 10 in. in width by 17-3/4 in. in length by 20 in. in height. The material used is Type 6061 aluminum, 1/2 in. thick. The tank has been hard-anodized to reduce corrosion. The core is surrounded on all sides (except the side facing the pulsed neutron source) with 1/2-in. -thick borated polyethylene (28 wt-% boron). The side facing the pulsed neutron source is covered with a 1/8-in. thickness of the same material. The top of the core is covered with 1/2-in. -thick 20 wt-% borated glass. The core tank is secured to the support table with bolts and a rubber gasket is used as a water seal. The tank is filled by means of a variable-speed pump continuously adjustable to a maximum flow rate of about 6 gal/min. A 2-in. solenoid-operated dump valve would drain the core in about 17 sec in case of a power failure or scram.

A movable boundary, constructed from a 1/2-in. -thick aluminum plate with 15 mils of cadmium bonded to it, allows the thickness of the core to be varied. The boundary is backed with sheets of borated polyethylene to provide structural strength in the core and to ensure thermal-neutron absorption in the moderator beyond the boundary. Lucite spacers (0.125 in. by 0.250 in. by 18 in.) are used to prevent bowing of the fuel plates and to maintain a 0.125-in. water gap between the plates. A thin-walled aluminum tube, hereafter referred to as the "glory hole," with an inside diameter of 0.45 in., passes through the center of the core axially and is used in measuring neutron spectra, fluxes, and decay constants.

The fuel elements are slipped into 0.026-in. grooves cut into each end of the core tank with a 0.125-in. space between each two grooves.

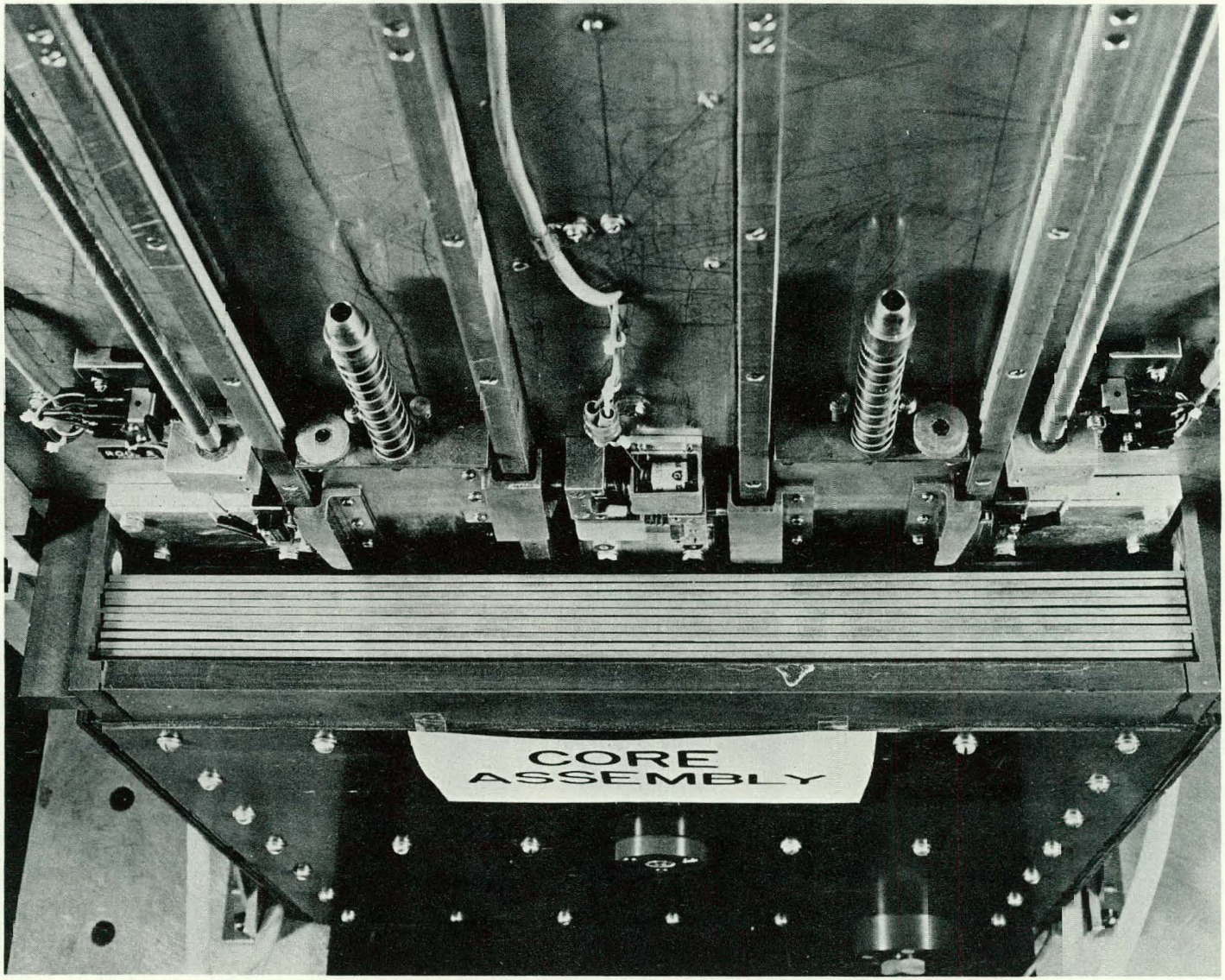

Fig. 2--Top view of the subcritical core and safety-rod assembly

2.2. FUEL ELEMENTS

The fuel plates for the assembly are made of uranium–aluminum alloy and are 18 in. long by 6 in. wide by 0.020 in. thick. They are about 16.86 wt-% uranium, 93.24% enriched in U^{235}. The plates are coated on each side with about 1 mil of clear Krylon plastic to reduce corrosion and minimize fission-product escape.

The average amount of U^{235} per fuel plate is 17.12 g and the mean is 17.15 g. The weights of the fuel plates were divided into three equal groups: high, low, and medium. For the loading program, the fuel plates near the average weight were chosen for the central portion of each slot, i.e., around the glory hole. The other two groups, the high and low groups, were then used alternately for the top and bottom position of each slot. Three fuel plates were placed in each slot for a total U^{235} content of three times the average weight, or 51.36 g. For 46 slots, the average weight of U^{235} per slot was 51.41 g, with the maximum and minimum weights per slot being 51.63 and 51.24 g, respectively. The maximum and minimum amounts of U^{235} per fuel plate used were 17.54 and 16.70 g, respectively.

2.3. SUPPORT TABLE

The support table is constructed of aluminum and is capable of holding 5 tons. The table is designed to support the subcritical assembly, including the necessary shielding for protection of personnel. The table is portable and may be raised or lowered by motor-driven jacks.

2.4. SAFETY-ROD ASSEMBLY

Two safety rods are used in the subcritical assembly as a fast shutdown mechanism. The time required for manual drop of each rod was measured to be 250 millisec. When the scram was initiated through the electronic circuitry, the time for rod drop was measured to be 340 millisec. The rods are suspended vertically over the core and are constructed from

cadmium encapsulated in stainless steel. Loose-fitting nylon bearings are used to guide the rods into the core. The rods are each 2-1/2 in. by 12 in. by 0.132 in. and are inserted into the core between two of the fuel elements.

2.5. SAFETY INSTRUMENTATION

The control console is shown in Fig. 3. The safety instrumentation consists of two independent neutron-current channels and a log count-rate channel. The neutron-current channels use gamma-compensated ion chambers and micromicroammeters. The log count-rate circuit is fed by a fission counter. The log count-rate circuit incorporates a recorder that provides a permanent record of the performance of the assembly by tracing a curve proportional to the logarithm of the neutron flux, which, when differentiated, amplified, and displayed on the period meter relay, gives the period of the assembly.

The compensated ionization chambers and fission counter are used to determine the multiplication of the core during the initial approach to full multiplication. The fission counter is centered directly below the core. The two ionization chambers are located directly below and parallel to the axial dimensions of the core. Each chamber is located on an opposite side of the center of the core and is positioned halfway between the center and an edge of the core.

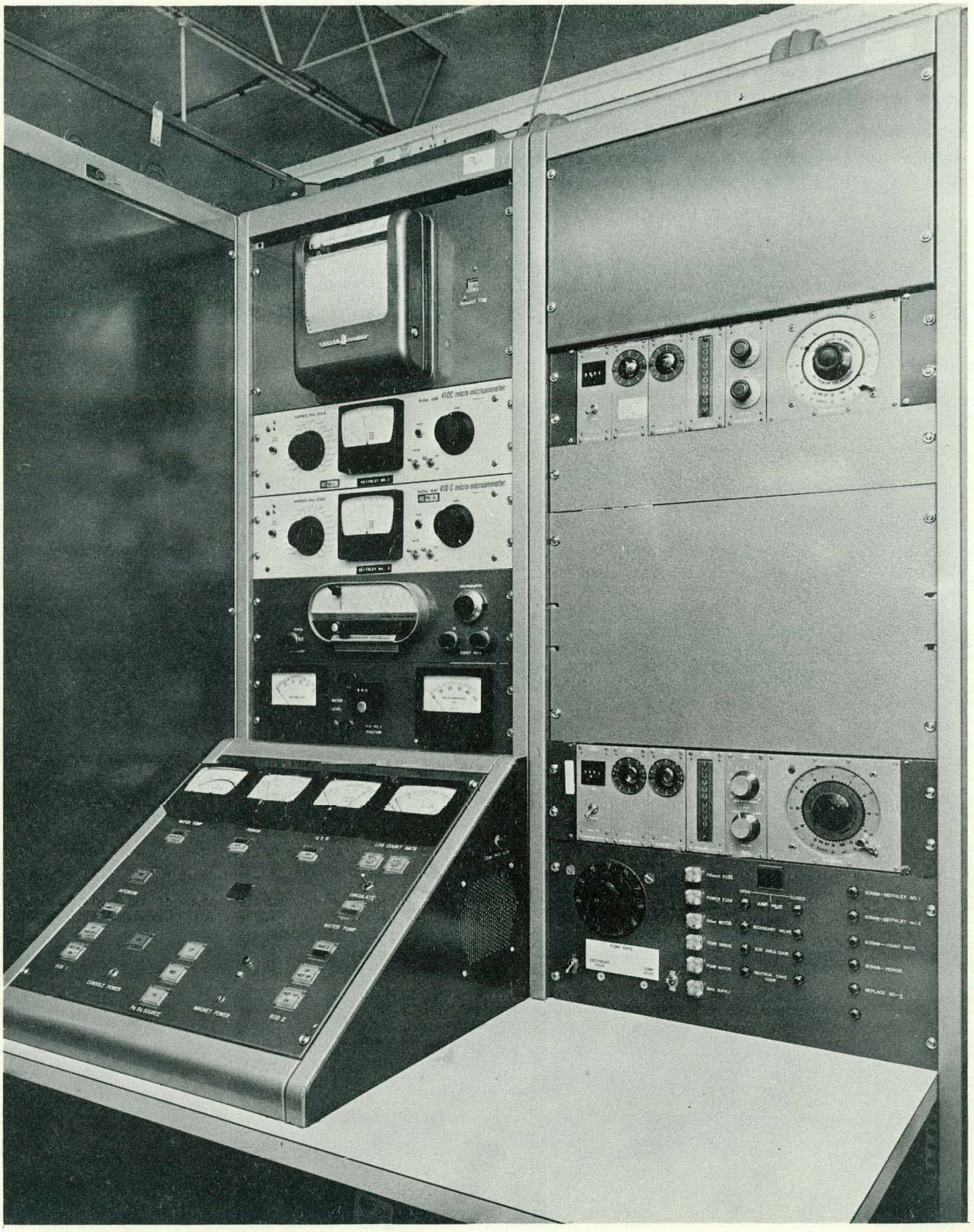

Fig. 3--Control console for the subcritical assembly

III. THEORY FOR ANALYSIS OF DATA

3.1. DECAY OF NEUTRON PULSE

For this study, theoretical expressions describing the time dependence of the neutron behavior in a pulsed multiplying assembly were generated. The procedure which has been adopted is to attempt a description using a two-group (slow- and fast-neutron groups) theory. The theoretical expression thus obtained will be compared with experiment in Section V. Before the derivations are given, the following definition of terms is necessary:

ϕ_s, ϕ_f	Slow and fast fluxes, respectively
v_s, v_f	Slow and fast velocities, respectively
Σ_{as}	Macroscopic absorption cross section, slow group
Σ_{tf}	Macroscopic fast transfer cross section into slow group
D_s	Diffusion constant, slow group
ν	Average neutron yield per fission
β	Effective delayed neutron fraction
τ	Age to indium resonance
P_f	Fast nonleakage probability
Σ_{fs}	Macroscopic fission cross section, slow group
K_n	Effective criticality constant for n^{th} spatial harmonic.

The two-group diffusion equations, including leakage, are then given by

$$\frac{1}{v_s}\left(\frac{d\phi_s}{dt}\right) = -\Sigma_{as}\,\phi_s + \Sigma_{tf}\,\phi_f + D_s\nabla^2\,\phi_s\ , \tag{1}$$

$$\frac{1}{v_f}\left(\frac{d\phi_f}{dt}\right) = -\Sigma_{tf}\,\phi_f + \nu\Sigma_{fs}\,(1-\beta)\,P_f\,\phi_s\ . \tag{2}$$

It is important to notice a subtlety introduced in Eq. (2), namely,

that of depleting the fast source by leakage before inserting its contribution into the fast group. If one does not do this, but merely adds a term $D_f \nabla^2 \phi_f$ in Eq. (2) to account for leakage, one will find that the fast lifetime to the thermal group depends on leakage, which is physically unrealistic. In the above formulation this is not true. One then solves the equations simultaneously after making a modal expansion in the spatial distribution as follows:

$$\phi_s = \sum_n e^{-\alpha_n t} R_n(x, y, z)\, \phi_{sn} \,, \tag{3}$$

$$\phi_f = \sum_n e^{-\alpha_n t} R_n(x, y, z)\, \phi_{fn} \,, \tag{4}$$

where $R_n(x, y, z)$ are an orthogonal set of functions satisfying the Helmholz equation and α_n is the decay constant for a particular mode.

For the geometry being used,

$$\nabla^2 R_n(x, y, z) = -B_n^2 R_n(x, y, z) \,. \tag{5}$$

Introducing Eqs. (3), (4), and (5) into Eqs. (1) and (2) and solving for a typical mode n, one gets

$$-\frac{\alpha_n}{v_s} \phi_{sn} R_n(x,y,z) = -\Sigma_{as} R_n(x,y,z)\, \phi_{sn} + \Sigma_{tf} R_n(x,y,z)\, \phi_{fn} - D_s \phi_{sn} B_n^2 R_n(x, y, z) \,, \tag{6}$$

$$-\frac{\alpha_n}{v_f} \phi_{fn} R_n(x,y,z) = -\Sigma_{tf} R_n(x, y, z)\, \phi_{fn} + \nu\Sigma_{fs}(1 - \beta) P_{fn} R_n(x, y, z)\, \phi_{sn} \,. \tag{7}$$

When ℓ_{sn}, ℓ_f, and K_n are defined as follows:

$$\ell_{sn} = \frac{1}{(\Sigma_{as} + D_s B_n^2) v_s} \,, \tag{8}$$

$$\ell_f = \frac{1}{v_f \Sigma_{tf}} \,, \tag{9}$$

$$K_n = \frac{\nu\Sigma_{fs} P_{fn}}{(1 + L_s^2 B_n^2)\Sigma_{as}}, \tag{10}$$

then

$$-\alpha_n \phi_{sn} = -\frac{\phi_{sn}}{\ell_{sn}} + \Sigma_{tf}\, \phi_{fn}\, v_s \tag{11}$$

$$-\alpha_n \phi_{fn} = -\frac{\phi_{fn}}{\ell_f} + \frac{(1 - \beta)\, \phi_{sn} K_n}{\ell_{sn}} \left(\frac{v_f}{v_s}\right) . \tag{12}$$

Eliminating ϕ_{sn} and ϕ_{fn} between Eqs. (11) and (12), one obtains the useful relationship

$$(1 - \alpha_n \ell_{sn})(1 - \alpha_n \ell_f) = K_n(1 - \beta) . \tag{13}$$

Equation (13) can be solved for α_n, giving the following two roots:

$$\alpha_n^{\pm} = \frac{\ell_n}{2\ell_{sn}\ell_f} \pm \sqrt{\frac{\ell_n^2}{4\ell_{sn}^2\ell_f^2} + \frac{K_n(1 - \beta) - 1}{\ell_{sn}\ell_f}} , \tag{14}$$

where $\ell_n = \ell_{sn} + \ell_f$.

An equally useful expression for the die-away (τ_n) is

$$\tau_n = \frac{1}{\alpha_n} = \frac{\ell_n}{2[K_n(1 - \beta) - 1]} \left(1 \pm \sqrt{1 + \frac{4\ell_{sn}\ell_f}{\ell_n^2}\,[K_n(1 - \beta) - 1]}\right). \tag{15}$$

Using the above derivations it is possible to make predictions of the experimental pulsed behavior of a multiplying assembly given the relative amplitudes of the spatial modes. Invoking the following initial boundary conditions on the thermal and fast fluxes:

$$\phi_s = 0 \qquad \text{at } t = 0$$

$$\phi_f = Q_n \qquad \text{at } t = 0 ,$$

one can rewrite Eqs. (3) and (4) as

$$\phi_s = \sum_n \phi_{sn} R_n(x,y,z)\left(e^{-\alpha_n^- t} - e^{-\alpha_n^+ t}\right), \tag{16}$$

$$\phi_f = \sum_n \phi_{fn} R_n(x,y,z)\left(e^{-\alpha_n^- t} - e^{-\alpha_n^+ t}\right)$$

$$+ \sum_n Q_n R_n(x,y,z)\, e^{-\alpha_n^+ t} . \tag{17}$$

Introducing Eqs. (16) and (17) into Eq. (1), one obtains two equations interrelating ϕ_{sn}, ϕ_{fn}, and Q_n:

$$-\alpha_n^- \phi_{sn} + \frac{\phi_{sn}}{\ell_{sn}} - \frac{\phi_{fn}}{\ell_f}\left(\frac{v_s}{v_f}\right) = 0 \tag{18}$$

$$+\alpha_n^+ \phi_{sn} - \frac{\phi_{sn}}{\ell_{sn}} + \frac{\phi_{fn}}{\ell_f}\left(\frac{v_s}{v_f}\right) - \frac{Q_n}{\ell_f}\left(\frac{v_s}{v_f}\right) = 0 . \tag{19}$$

From Eq. (18),

$$\phi_{sn}(1 - \ell_{sn}\alpha_n^-) = \frac{\ell_{sn} v_s}{\ell_f v_f}\,\phi_{fn} . \tag{20}$$

Substituting Eq. (20) into Eq. (19) and solving for ϕ_{fn}, one obtains

$$\phi_{fn} = \frac{Q_n(1 - \ell_{sn}\alpha_n^-)}{\ell_{sn}(\alpha_n^+ - \alpha_n^-)} . \tag{21}$$

From Eq. (20),

$$\phi_{sn} = \frac{Q_n v_s}{(\alpha_n^+ - \alpha_n^-) v_f \ell_f} . \tag{22}$$

The above relationships are used in Section V to explain the behavior of the observed spatially independent die-away measurements.

3.2. NEUTRON SPECTRA

The theoretical methods of analysis used in evaluating the spectra measurements were essentially those developed under Project Agreement No. 2. The neutron balance equation in diffusion approximation was solved numerically. This equation is

$$-D(E)\,\nabla^2\phi(E,x) + \Sigma_T(E)\phi(E,x) = \int_0^{E_m} \phi(E',x)\Sigma(E' \rightarrow E)dE' + \theta(E,x) \quad . \quad (23)$$

The terms in this equation are defined as follows:

$D(E)$	Diffusion coefficient for water
$\phi(E,x)$	Neutron flux
$\Sigma_T(E)$	Macroscopic total cross section
$\Sigma(E' \rightarrow E)$	Energy transfer kernel
$\theta(E,x)$	Epithermal source (neutrons scattered to energy E from above E_m)
E_m	Thermal cutoff energy, i.e., that energy above which there are no effects of chemical binding and no upscattering.

If one separates space and energy in the usual way,

$$\begin{aligned} \theta(E,x) &= S(E)R(x) \\ \phi(E,x) &= \phi(E)R(x) \quad , \end{aligned} \qquad (24)$$

and introduces the localized buckling at the point of measurement defined as follows:

$$\frac{\nabla^2 R(x)}{R(x)} = -B^2 \quad , \qquad (25)$$

one obtains

$$[D(E)B^2 + \Sigma_T(E)]\ \phi(E) = \int_0^{E_m} \phi(E')\Sigma(E' \rightarrow E)dE' + S(E) \quad , \qquad (26)$$

which can be solved using the standard computer codes SPECTRUM or DESMOS. Spectra calculated from this method are used in Section V for comparison with the measured spectra.

IV. PREVIOUS CALCULATIONS

4.1. REACTIVITY CALCULATIONS

The reactivity calculations made prior to loading of the subcritical assembly were based on an empirical method [2][3] for calculating the critical thickness of homogeneous, highly enriched uranium–hydrogen assemblies, bare and reflected. The method utilizes an empirical buckling and an extrapolation distance, B_o^2 and λ_o, respectively. The nomenclature has been changed from the customary to prevent confusion between the empirical terms and the standard terms. In the empirical method, a function $f(B_o)$ is defined which provides a relationship between B_o^2 and the moderator-to-fuel ratio (H/U).

With the subcritical assembly assumed to have plates 0.020 in. by 18 in. by 6 in. with about 17 g of U^{235} per plate, curves were constructed (shown in Fig. 4) of H/U versus the following: A, the bare or reflected critical thickness; δ_o, the reflector savings plus the extrapolation distance; B_o^2; λ_o; and ρ, the density of U^{235}. It was further assumed that the subcritical assembly was homogeneous and that the empirical method, which considers only hydrogen and U^{235}, was applicable to the uranium–aluminum and water subcritical assembly.

The critical B_o^2 given by the empirical method and the one-group criticality equation,[4]

$$K_{eff} = \frac{K_\infty e^{-\tau B_o^2}}{1 + L^2 B_o^2} , \qquad (27)$$

were used to obtain a value of τ which satisfied Eq. (27) at $K_{eff} = 1$. For calculating more exactly the core thicknesses which yielded K_{eff}'s < 1, the

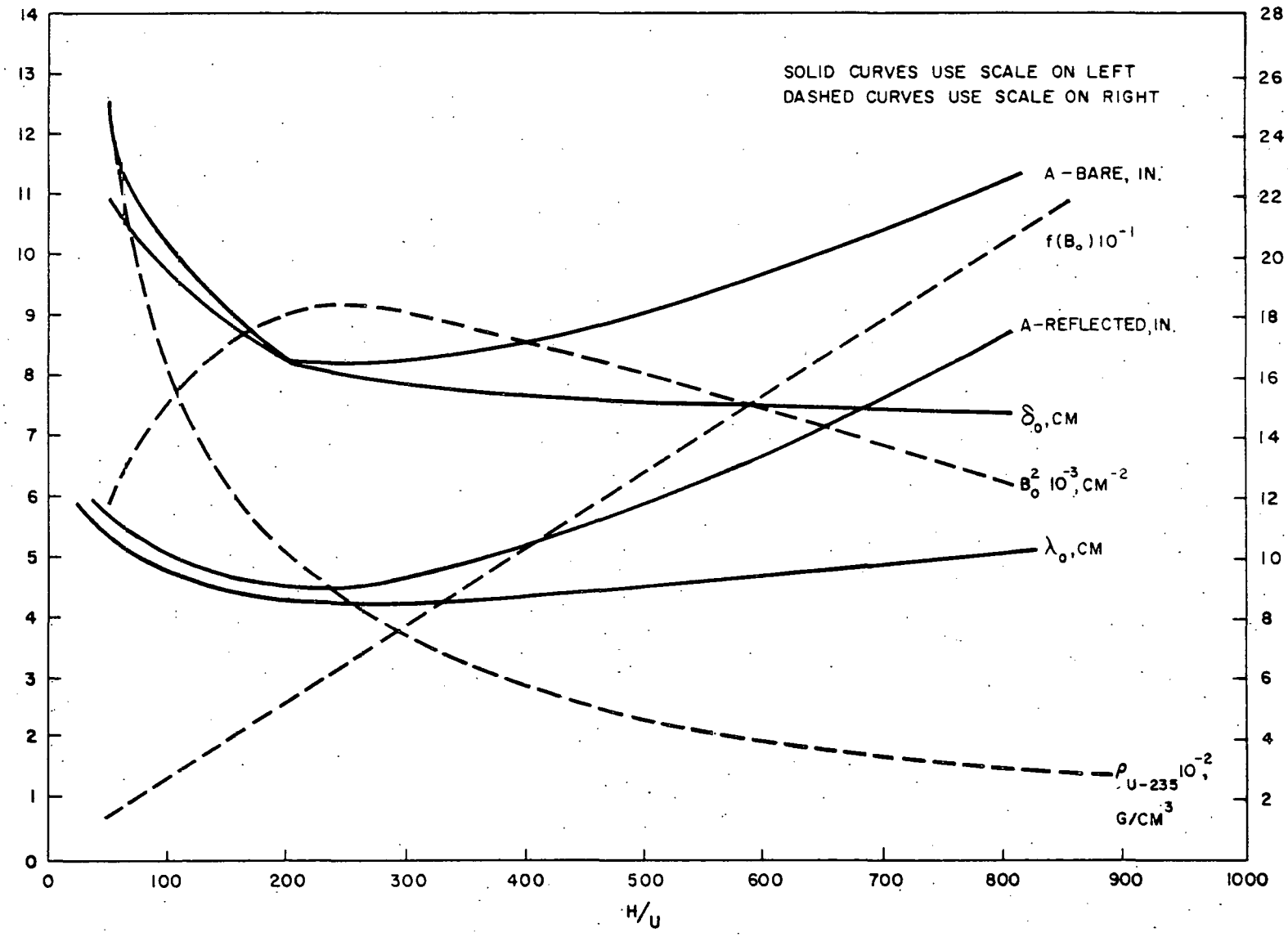

Fig. 4--Critical values calculated using the empirical method

ratio of the criticality equation, Eq. (27), for $K_{eff} = 1$ to that for K_{eff}'s < 1 was used. This ratio, with some simplifications, yields

$$K_{eff} \cong e^{-\Delta B^2 \tau}(1 - L^2 \Delta B^2), \qquad K_{eff} < 1 , \tag{28}$$

where $\Delta B^2 = B_1^2 - B_0^2$. To obtain the value of λ_1 to be used in the calculation of B_1^2, it was assumed that the critical empirical relation $3\lambda^2 B^2 = 1$ was appropriate. The results of these calculations are shown in Fig. 5.

Using the same method for calculating $K_{eff} < 1$, a curve of K_{eff} and the reactivity, ρ, versus the height of water in the bare multiplying assembly was constructed; this curve is shown in Fig. 6. The final water height attainable in the assembly was 18 in., but the calculations were made for heights in excess of this. Since the exposed plates have only a small effect, they were ignored for this calculation.

It is possible to estimate the resulting period if it is assumed that water is inserted into the core at a slow rate. The equation which was adopted to calculate the subcritical period is given by Schultz[5] as

$$T = \frac{1 - K_{eff}}{dK_{eff}/dt}, \qquad K_{eff} < 1 . \tag{29}$$

This approximate equation gives a lower limit on the period. Assuming the water is inserted at 6 gal/min, the minimum period was calculated to be approximately 30 sec. No observable period was noted for any of the loadings.

An estimate of the worth of the safety rods to be used in the multiplying assembly was made. In this calculation, it was assumed that the worth of a rod is given by its statistical weight. The statistical weight of a region is defined[4] as

$$W(R) = \frac{\int_R \phi^2 \, dv}{\int_v \phi^2 \, dv}, \tag{30}$$

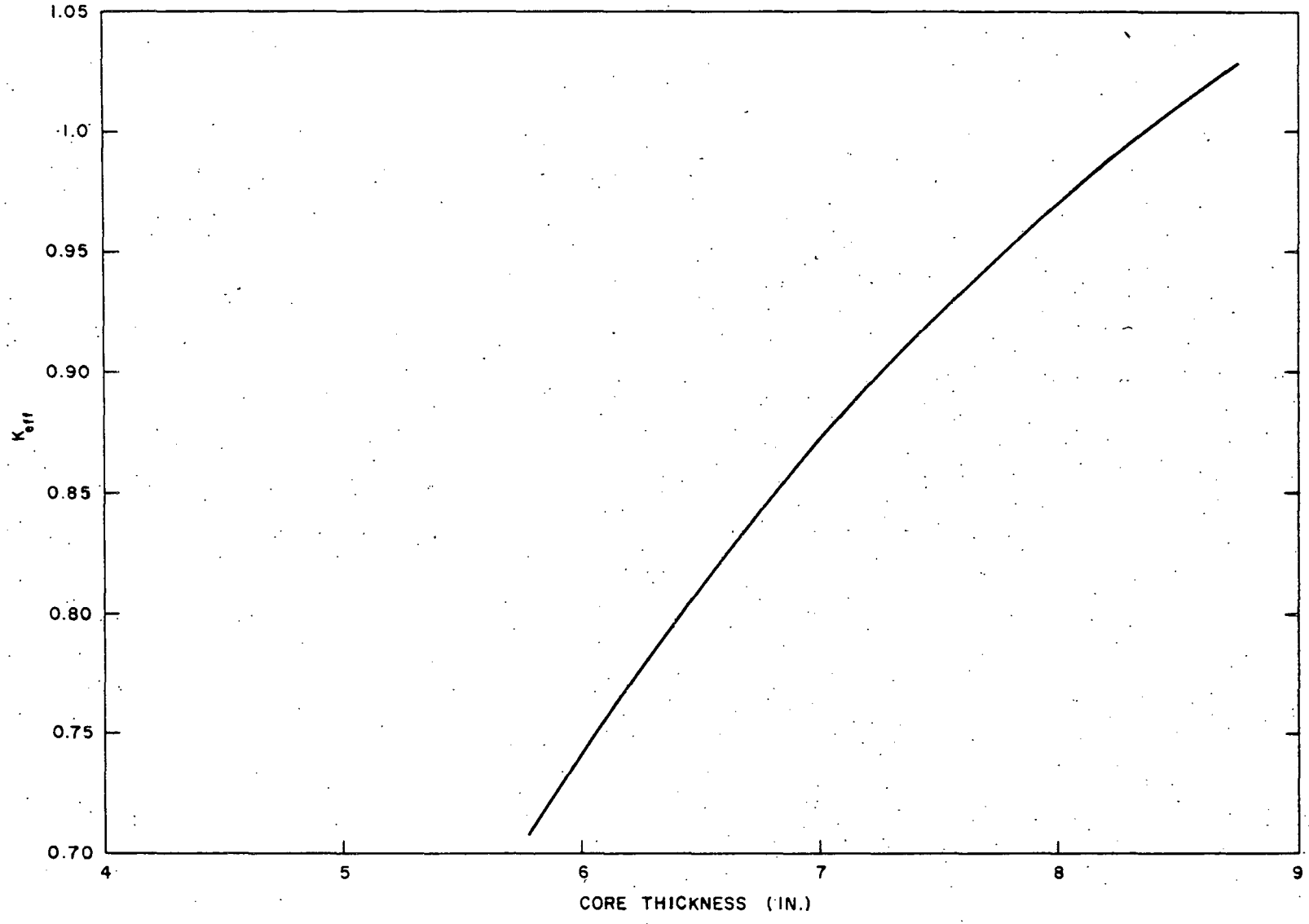

Fig. 5--K_{eff} as a function of bare-core thickness calculated using the empirical method

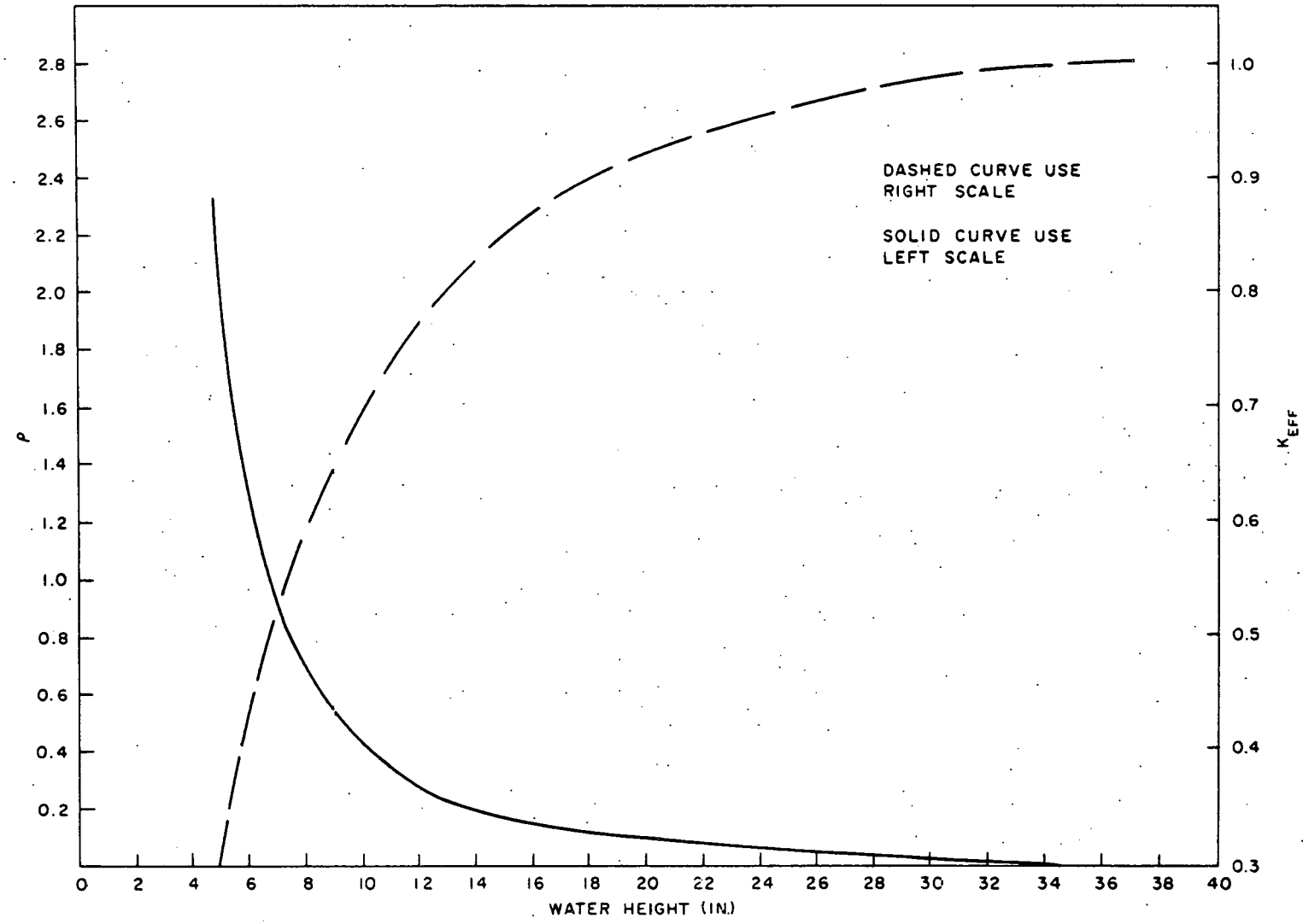

Fig. 6--Calculated values of reactivity and K_{eff} versus water height in a bare-core assembly

where the notation used is the same as that of Glasstone and Edlund. The equation used for evaluating the worth of a safety rod for the multiplying assembly was

$$\text{Safety rod worth} = \frac{\Delta K \int_b^9 \int_a^{a+T} \phi_0^2 \phi_1^2 \cos^2 \frac{\pi x}{18} \cos^2 \frac{\pi y}{18} \, dx dy}{\int_{-9}^9 \int_{-9}^9 \phi_0^2 \phi_1^2 \cos^2 \frac{\pi x}{18} \cos^2 \frac{\pi y}{18} \, dx dy}, \qquad (31)$$

where $(a + T) < 9$, $9 > b > -9$, and ΔK represents the worth of an 18-in. by 18-in. rod, which when fully inserted, constitutes a boundary.

Figure 7 shows the location of a safety rod in the assembly and defines the limits given in Eq. (31).

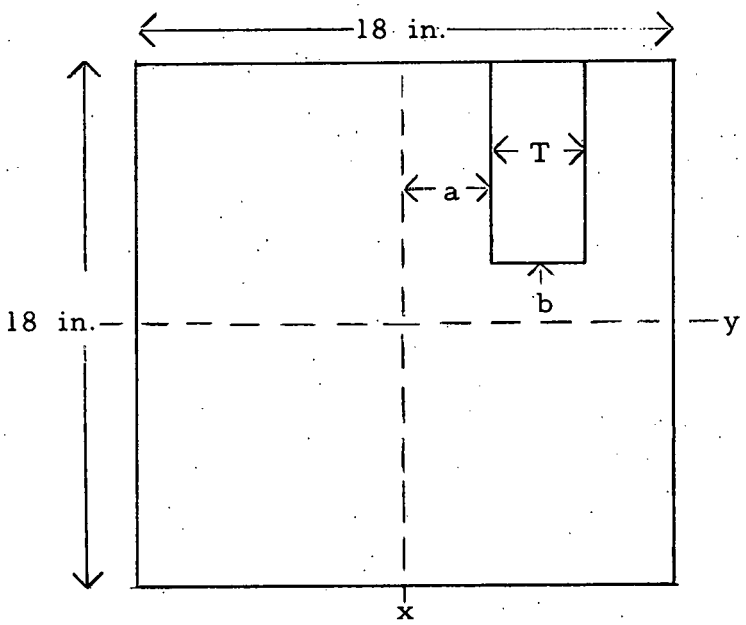

Fig. 7--Location of a safety rod in the x-y plane of the multiplying assembly

The worth of a single safety rod, for which a = 2.625 in., T = 2.5 in., and b = -3 in., located 2.5 in. in from an edge is calculated to be approximately $0.066\ \Delta K_{cff}$ for an assembly which has a multiplication of 10.

The period of the multiplying assembly during rod removal may be approximated by using Eq. (29), if one assumes that the rate of removal of the safety rod is slow and constant. If the removal rate is constant, b is a function of time, and dK_{eff}/dt may be evaluated for a given multiplication. The period (obtained using Eq. (29)) versus rod withdrawal is shown in Fig. 8. The withdrawal rate for the multiplying-assembly rods was 0.14 in./sec.

Reactor constants and experimental data are contained in Appendix A. The cross sections and constants which are tabulated are the ones which were used in all calculations concerning the multiplying assembly.

4.2. SHIELDING CALCULATIONS

In Appendix B, the following equation (Eq. (46)) was derived:

$$Ip(total) = 6.6 \times 10^{-10} Y \text{ r/hr} ,$$

This equation and values of Y taken from Ref. 6 were used to compute the decay rate of the subcritical assembly. This theoretical decay rate was normalized to the experimental data at a time after shutdown equal to 10^5 sec. The normalized theoretical and the experimental decay curves are shown graphically in Fig. 9.

In the first quarterly report,[7] a shielding calculation similar to that given in Appendix B was done, and a graph of this decay rate was presented in the second quarterly report.[8] The original assumptions made in the first quarterly report have been corrected to conform to actual operating conditions. The original assumptions and the corrections are as follows:

1. The core thickness was 10 in. It is actually 7 in.
2. The core would contain uranium–aluminum fuel plates and water when measurements on the core were made. Actually, the water moderator was not in the core and shielding was needed only when

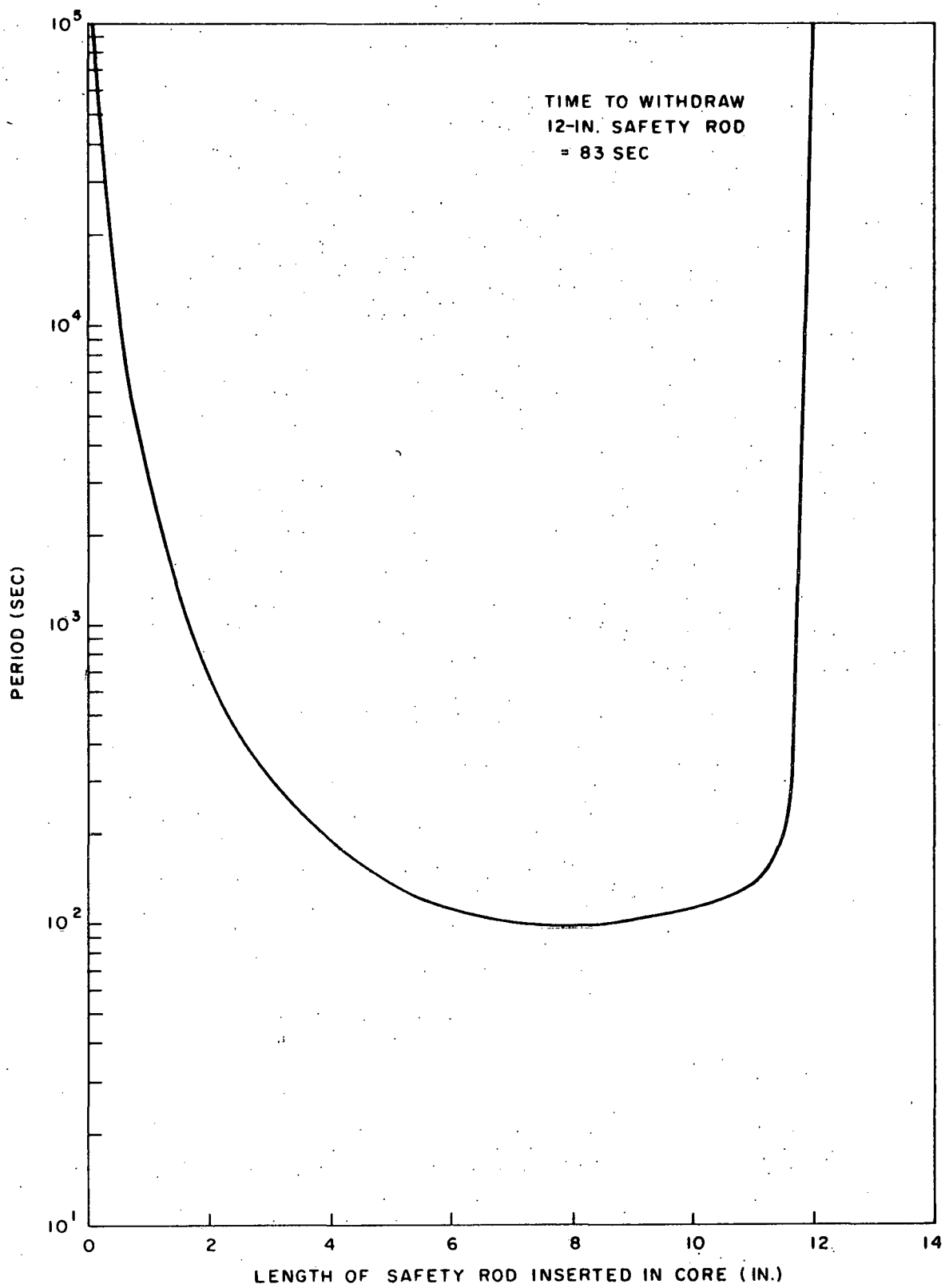

Fig. 8--Calculated value of period versus rod withdrawal at $K_{eff} = 0.9$

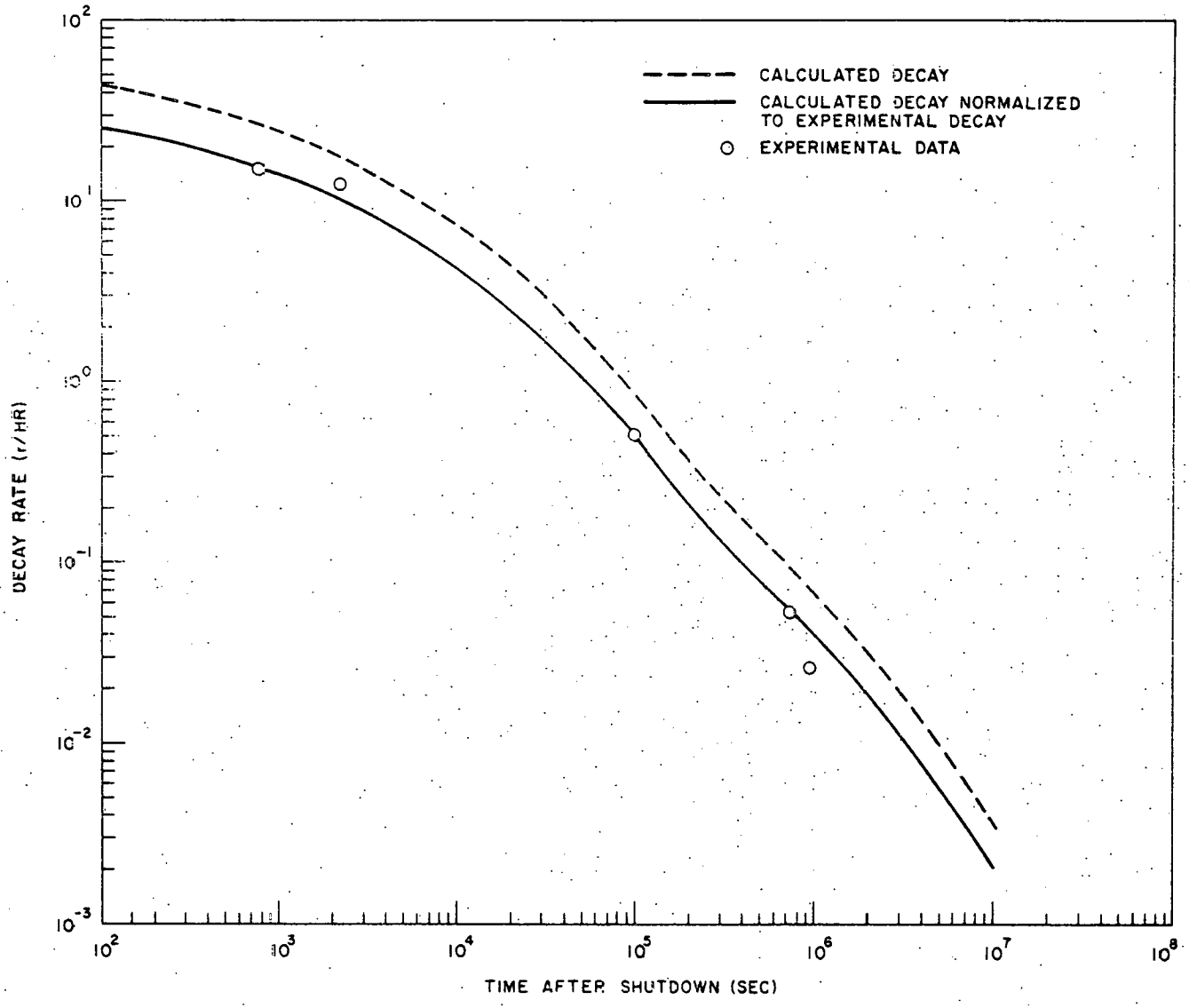

Fig. 9--Decay rate of activity in the core as a function of time

personnel entered the shielded neutron cave.

3. The assembly would be operated at a full power level for 1000 hr before shutdown. The assembly was actually operated about 11 hr at full power before shutdown.
4. The radiation level would be monitored at 6 in. from the midpoint of the 18-in. by 18-in. side of the assembly. It was measured at 3-1/2 in. from the 18-in. by 18-in. side of the assembly.

The effect of the original assumptions was such as to make the shielding calculations conservative.

As can be seen from Fig. 9, there is a reasonable agreement between the normalized calculated and experimental decay rates of the assembly. This normalized calculated decay curve can therefore be used in future work to predict in advance the radiation level of the assembly, assuming the geometry of the assembly and the relative position of the core and detector remain constant.

V. EXPERIMENTAL INVESTIGATIONS

All of the experiments carried out with the multiplying assembly were performed in the shielded neutron cave shown in Fig. 10. The assembly was located within the shielded neutron cave in the manner illustrated in Fig. 11.

5.1. INITIAL APPROACH TO FULL MULTIPLICATION

The approach to full multiplication was made in discrete steps. Each step consisted in slipping a predetermined number of fuel plates into consecutive grooves in the core tank, and securing the movable cadmium boundary. Then neutron-current measurements were taken at different water heights with the two ion chambers and count rates were taken with the fission counter described in Section II. Curves of the neutron currents, measured with the two ion chambers, versus the water height for the last loading are shown in Fig. 12. A 5-curie PoBe source was used for all multiplication measurements. The location of the PoBe source is shown in Fig. 11. The normal distance from the core to the source is 2-1/2 in. For these measurements, the source was positioned 6-1/4 in. above the table. Conventional inverse-multiplication plots were maintained and used to determine the actual loadings. The results of the multiplication plots are shown in Fig. 13. The two ion chambers seem to be located satisfactorily in relation to the PoBe source for approach-to-critical measurements. However, the fission counter appears to be too close to the PoBe source. Inverse-multiplication data from the two ion chambers indicate $K_{eff} = 0.85$ for the last loading. All but the first three loadings in this approach to full multiplication were determined from the inverse-multiplication curves.

Prior to the actual loading of the assembly with uranium–aluminum

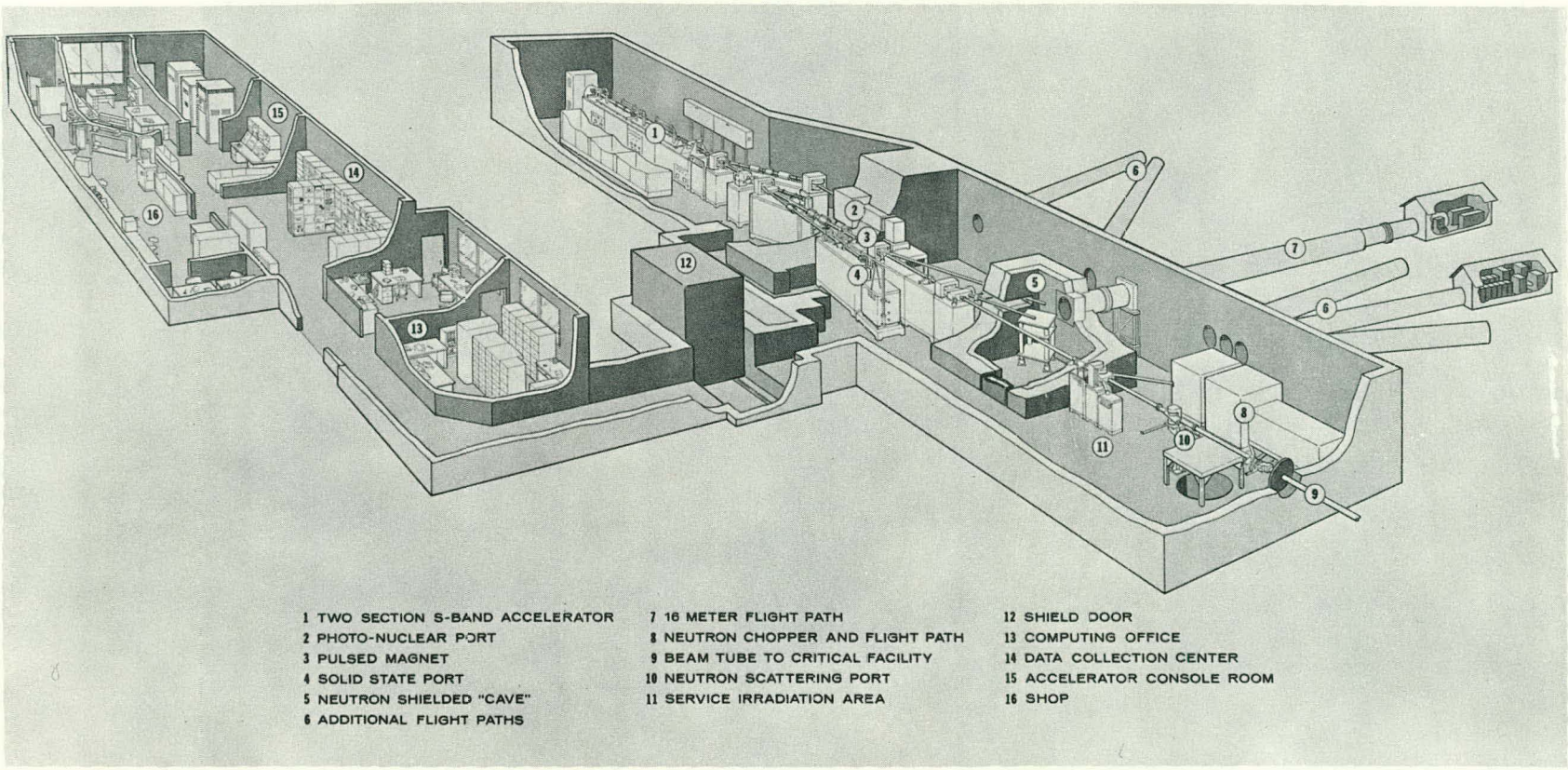

Fig. 10--General Atomic electron linear accelerator facility

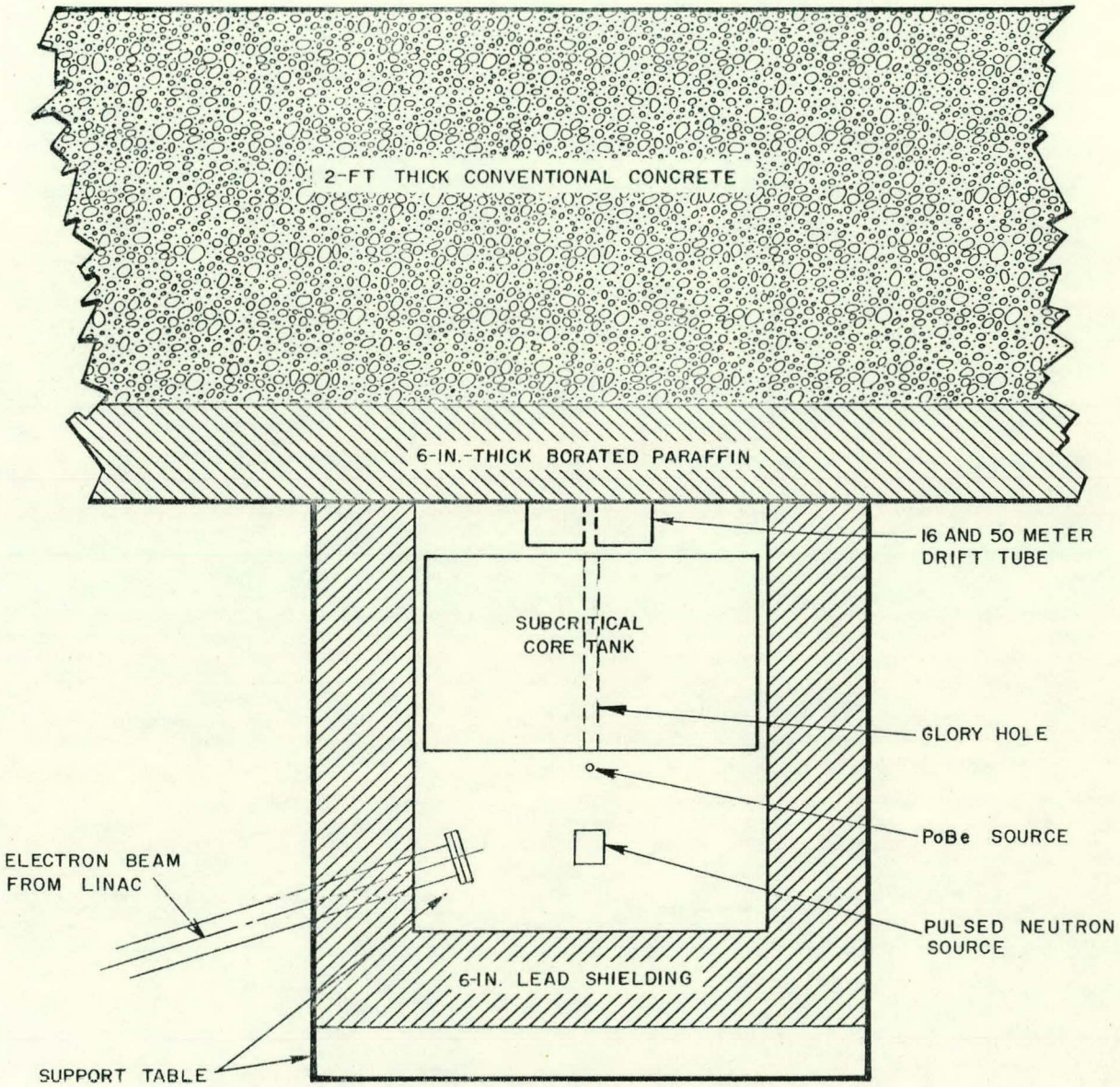

Fig. 11--Plan view showing geometry for measurements in the subcritical assembly

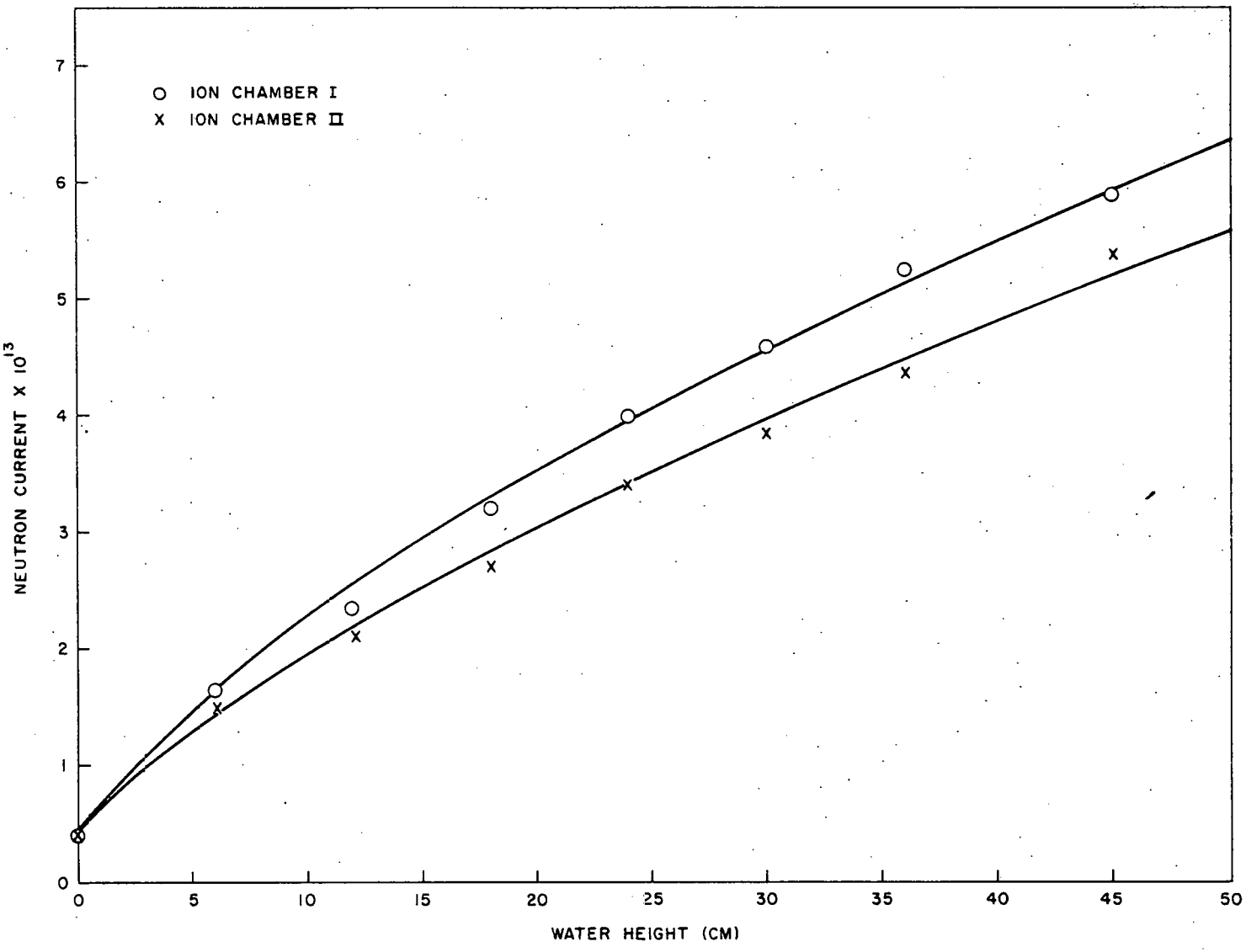

Fig. 12--Count rates versus water height for the last loading

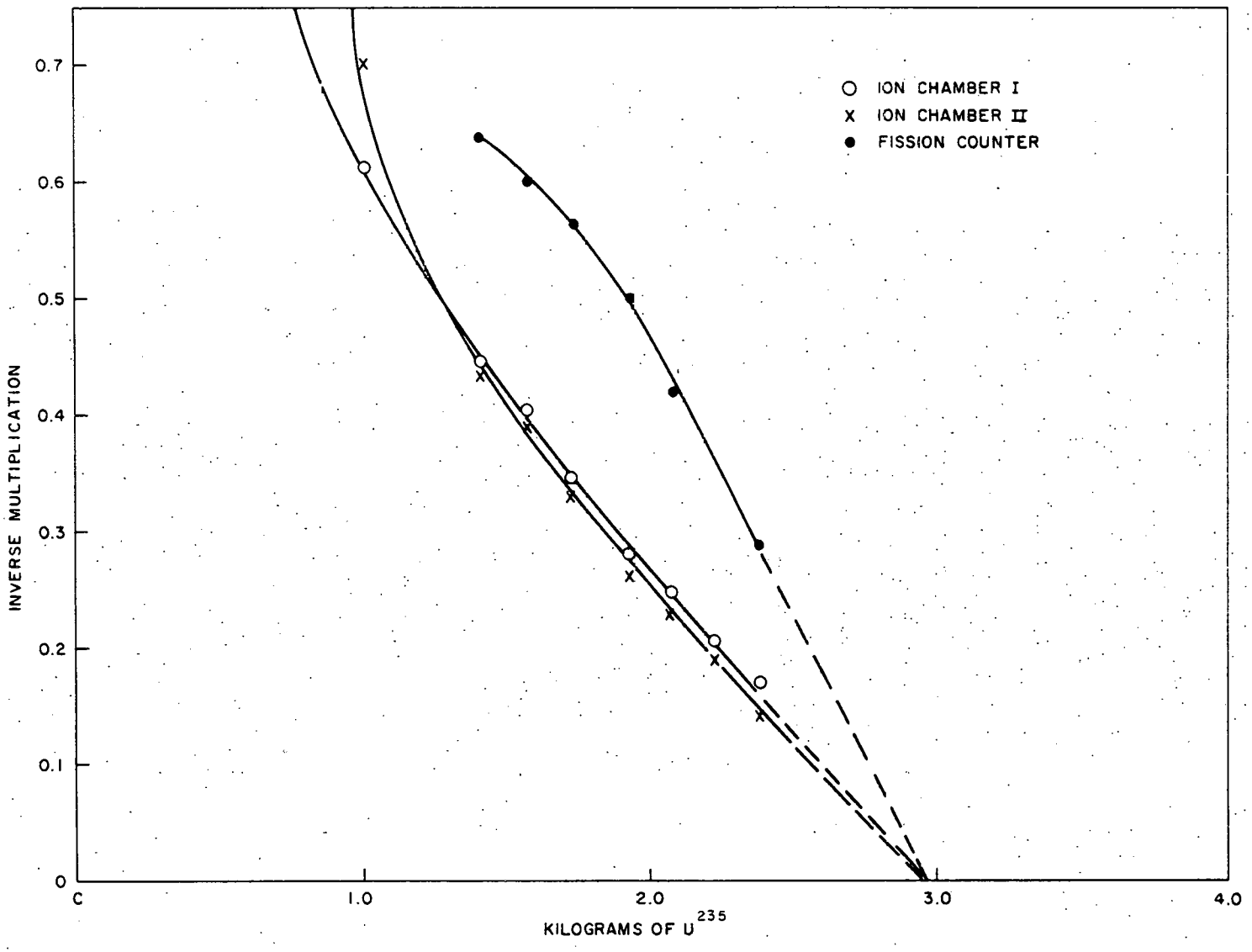

Fig. 13--Inverse multiplication versus kilograms of U^{235}

plates, borated-aluminum plates having the same thermal-neutron absorption characteristics as the uranium–aluminum plates were loaded into the core. The boron–aluminum plates were loaded in accordance with Table 1a and measurements similar to those with the uranium–aluminum plates were made at each step. The steps indicated in Table 1a were determined for U^{235} based on the calculated critical mass. The critical mass of the bare core assembly was calculated to be 2.9 kg of U^{235}. The mass of U^{235} to reach a K_{eff} of 0.9 was calculated to be 2.5 kg. The actual loadings made with the uranium–aluminum plates are given in Table 1b.

Table 1

LOADING SCHEDULE

Loading Number	Number of Fuel Plates	U^{235} per Loading (g)	Total U^{235} (g)
a. Calculated Loading			
1	30	510	510
2	30	510	1020
3	24	408	1428
4	18	306	1734
5	15	255	1989
6	12	204	2193
7	6	102	2295
8	6	102	2397
9	3	51	2448
10	3	51	2499
b. Actual Loading			
1	30	513.68	513.68
2	30	489.13	1002.81
3	24	411.46	1414.27
4	9	154.19	1568.46
5	9	154.08	1722.54
6	12	205.51	1928.05
7	9	154.21	2082.26
8	9	154.14	2336.40
9	9	154.15	2390.55

5.2. DIE-AWAY MEASUREMENTS

At each step in the approach, the decay constant for the subcritical assembly was determined. A fission counter (1/4 in. in diameter by 1/4 in. in active length) placed in the glory hole (see Fig. 11) was used to measure the time distribution of the thermal neutrons following a 0.5-μsec-wide pulse of fast neutrons in the core. For these measurements, the PoBe source was lowered into a shield below the table top. A typical decay curve for the last loading is shown in Fig. 14. The scattering of points around 4 millisec indicates the presence of the delayed-neutron groups. Measurements were made with and without the safety rods in the core for the last loading. Figure 15 shows the decay curves for these measurements. With Eq. (13) from Section III being used to determine K_{eff} from the decays with the rods in and the rods out, the total worth of the rods was indicated to be about 0.05 in. ΔK_{eff}. A single rod in the core was measured to be worth about 0.02 in. ΔK_{eff}. Calculations had indicated a single-rod worth of 0.066 in. ΔK_{eff}.

In order to measure the decay of the fundamental mode of the assembly at the last loading, a modal analysis was made in the core to eliminate spatial effects. This analysis was accomplished by measuring the time distributions of thermal neutrons every 1/2 in. along the glory hole. The computer code ORPHEUS was used to determine from the space points the Fourier coefficients for the different harmonics as a function of time. Figure 16 shows the time-space distribution of thermal neutrons in the core at the final loading following a 0.5-μsec burst of fast neutrons. The Fourier coefficients for the fundamental mode are shown in Fig. 17. The decay constant for the fundamental mode was measured to be 2.44×10^3 sec^{-1}. From Eq. (13) in Section III, this decay constant gives $K_{eff} = 0.91 \pm 0.02$. The error in K_{eff} was determined using the actual measured error in α and assuming an error of 50% in ℓ_f and 20% in ℓ_s. For the second harmonic, $K_{eff} = 0.23$ was obtained.

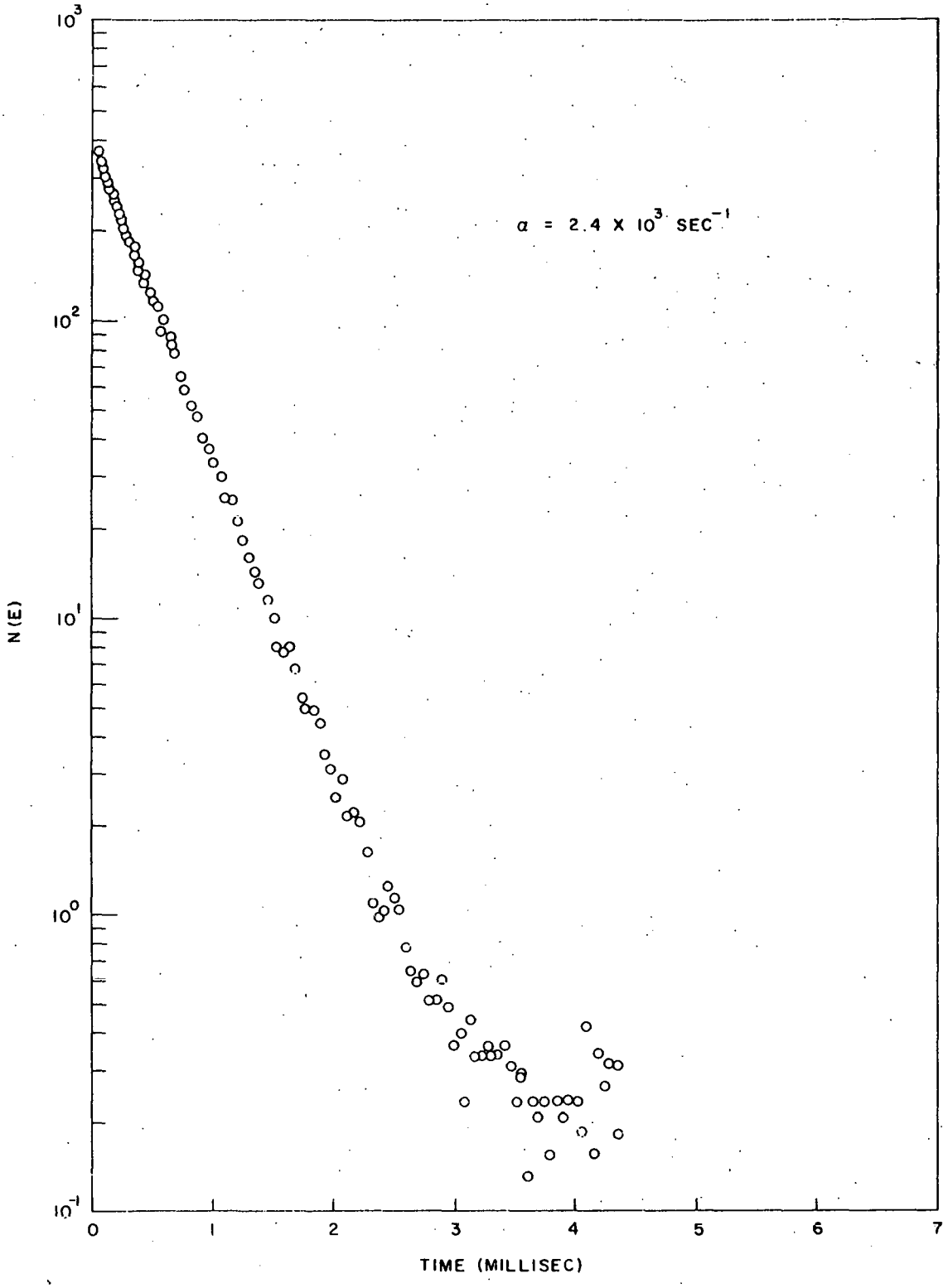

Fig. 14--Decay of thermal neutrons in the core after a 0.5-μsec burst of fast neutrons

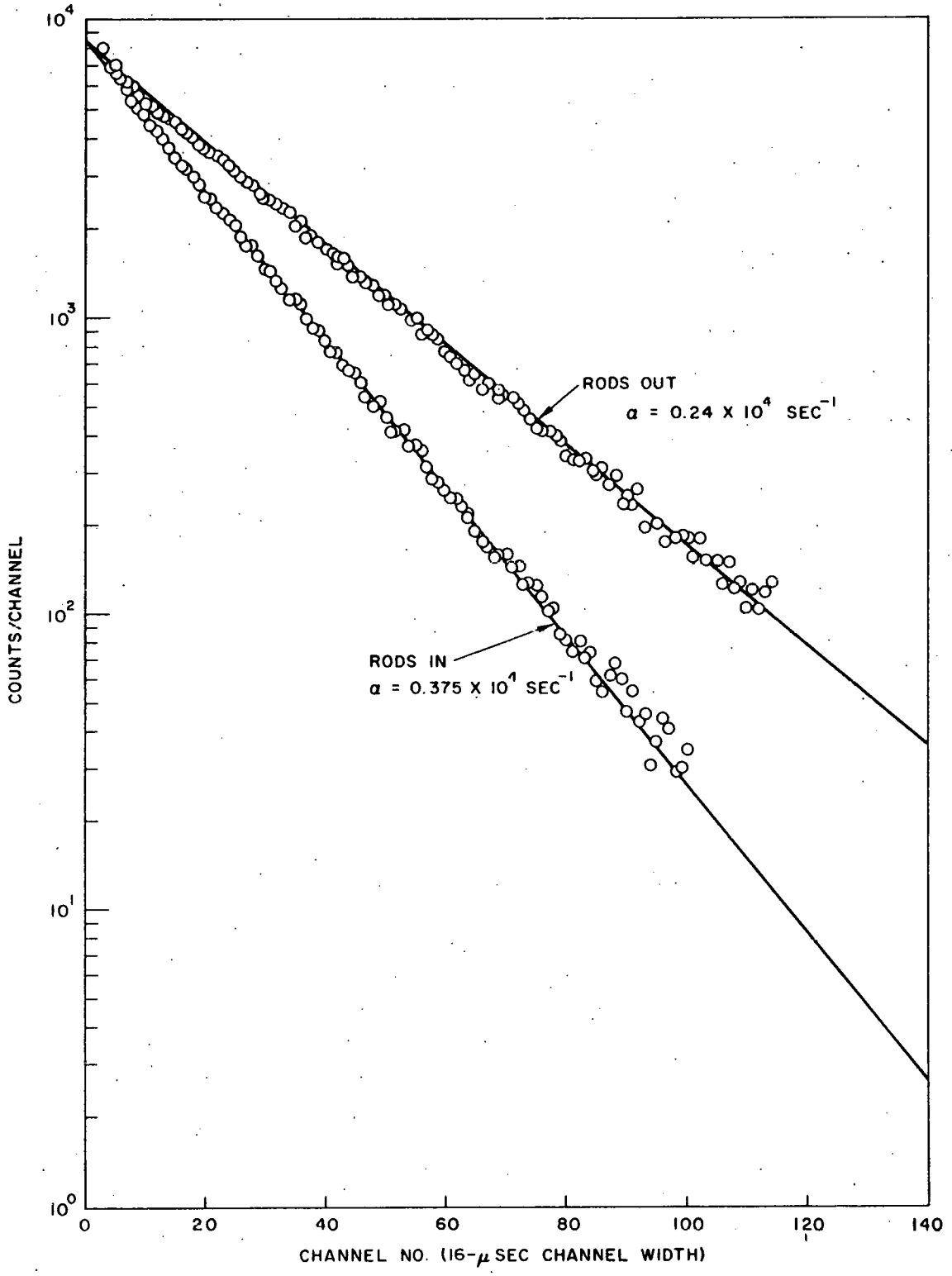

Fig. 15--Decay of thermal neutrons at the last loading with and without safety rods in the core

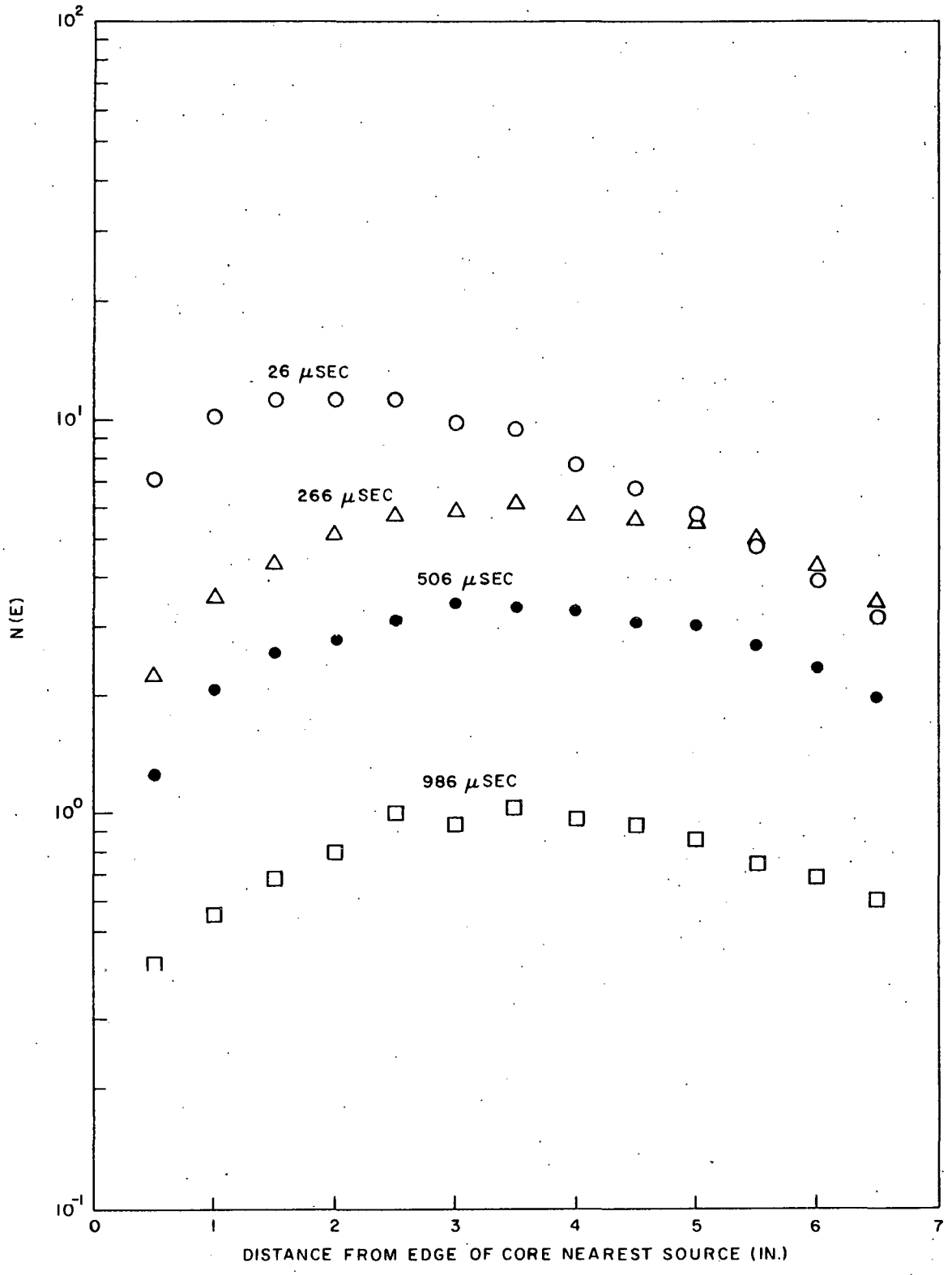

Fig. 16--Time-space distributions of thermal neutrons in the core following a 0.5-μsec burst of fast neutrons

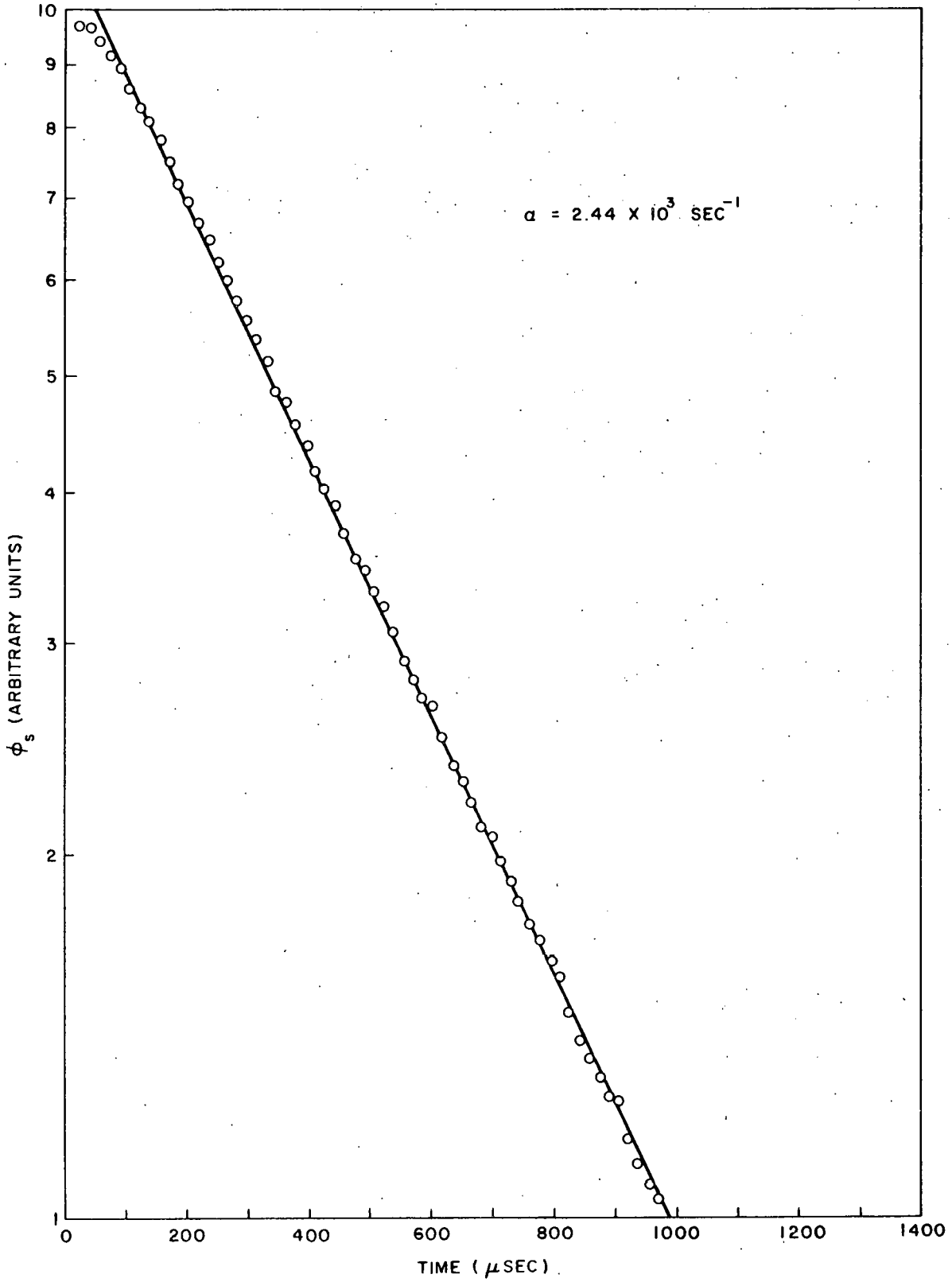

Fig. 17--Decay of the fundamental mode at the last loading

A buildup of the thermal neutrons is indicated in Fig. 17. An expanded view of the early times in Fig. 17 is shown in Fig. 18, where Eq. (16) for the fundamental mode is compared with the experimental data. Figure 19 shows the same comparison for the second harmonic.

At each step in the approach to full multiplication, the decay constant for the subcritical assembly was determined. The K_{eff}'s (versus kilograms of U^{235}) calculated from Eq. (13), Section III, using these decay constants, are shown in Fig. 20, in comparison with the K_{eff}'s calculated using the method outlined in Section IV. The data indicate that both curves are extrapolating to the same point.

Figure 21 shows the measured decay constants as a function of buckling. The buckling was determined using an extrapolation length of $0.71\bar{\lambda}_{tr}$. The solid curve shown was calculated from Eq. (14), Section III, with

$$\frac{K_{\infty}\, e^{-B^2\tau}}{1 + L^2B^2}$$

replacing K_n. A value of 27 cm^2 was used in the above expression for τ. The poor agreement between Eq. (14) and the measured points was improved by using the extrapolation length determined from the thermal-flux measurements to calculate the buckling. These results are shown in Fig. 22 and seem to indicate an even longer extrapolation length would give better agreement.

5.3. NEUTRON-SPECTRUM MEASUREMENTS

Neutron spectra in the assembly were measured using standard pulsed-beam techniques.[1] A pulsed beam of electrons from the linear accelerator was used to produce neutrons in a water-cooled lead target. Bremsstrahlung

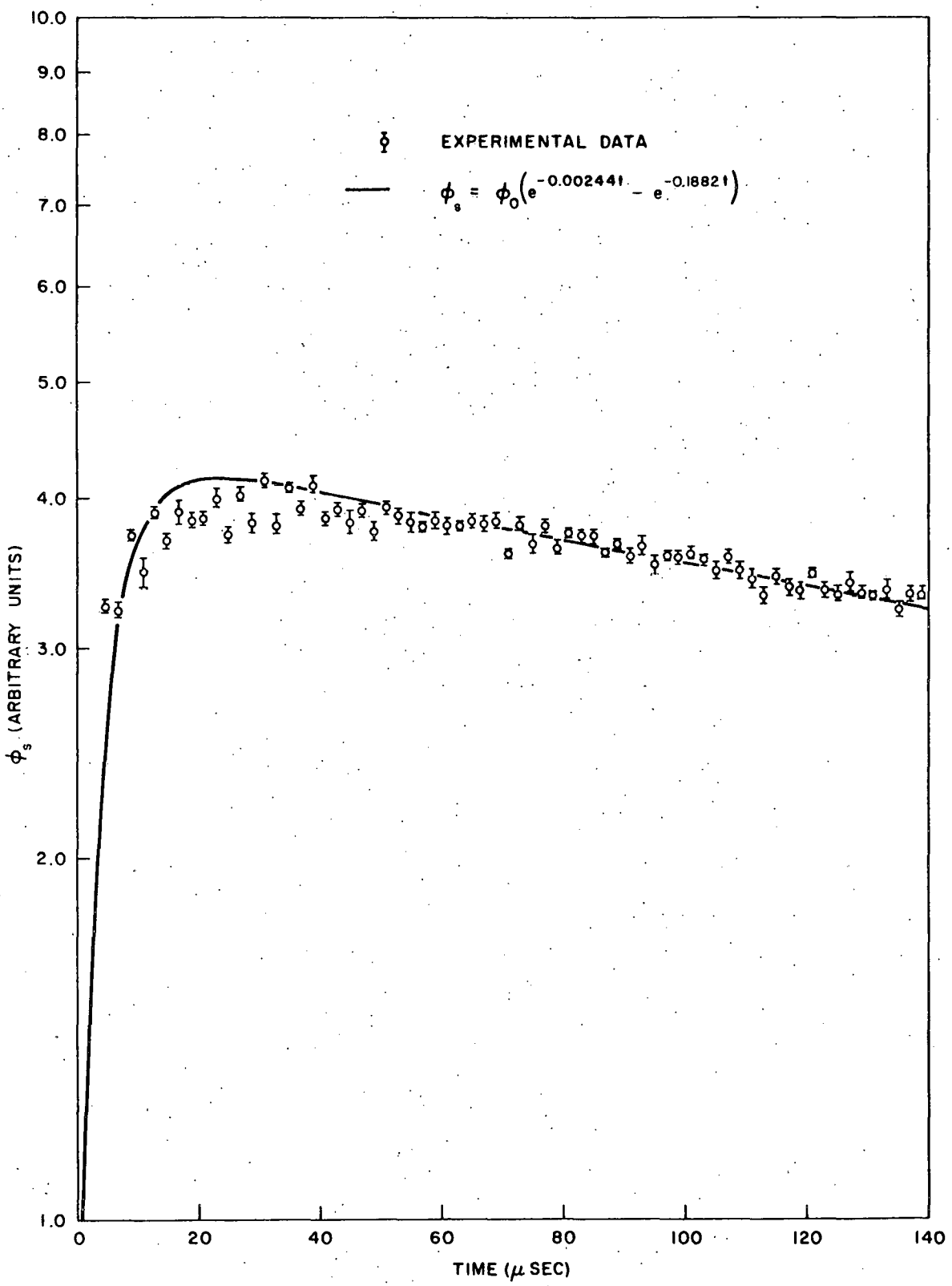

Fig. 18--Decay of the fundamental mode at early times for the last loading

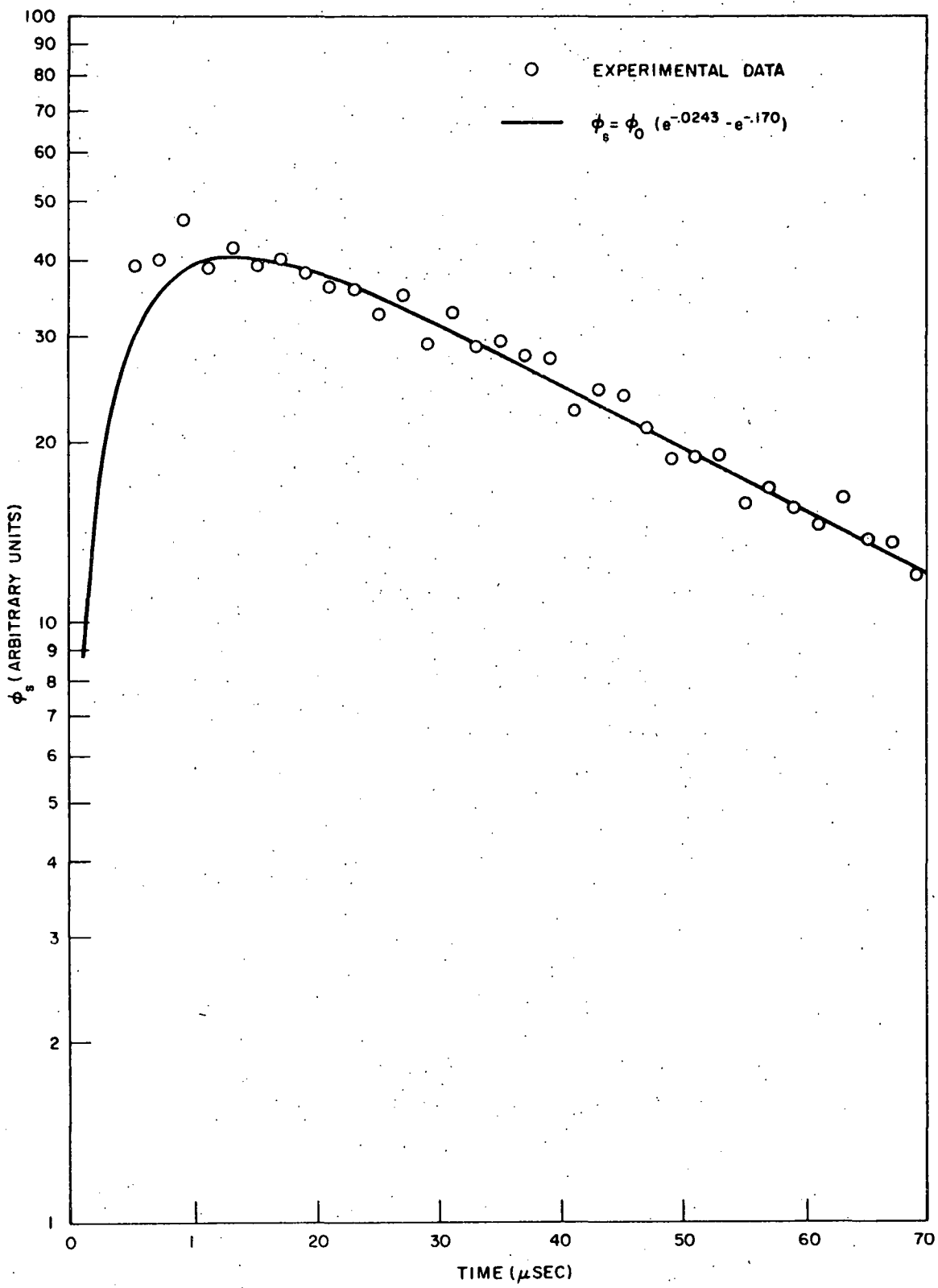

Fig. 19--Decay of the second harmonic at the last loading

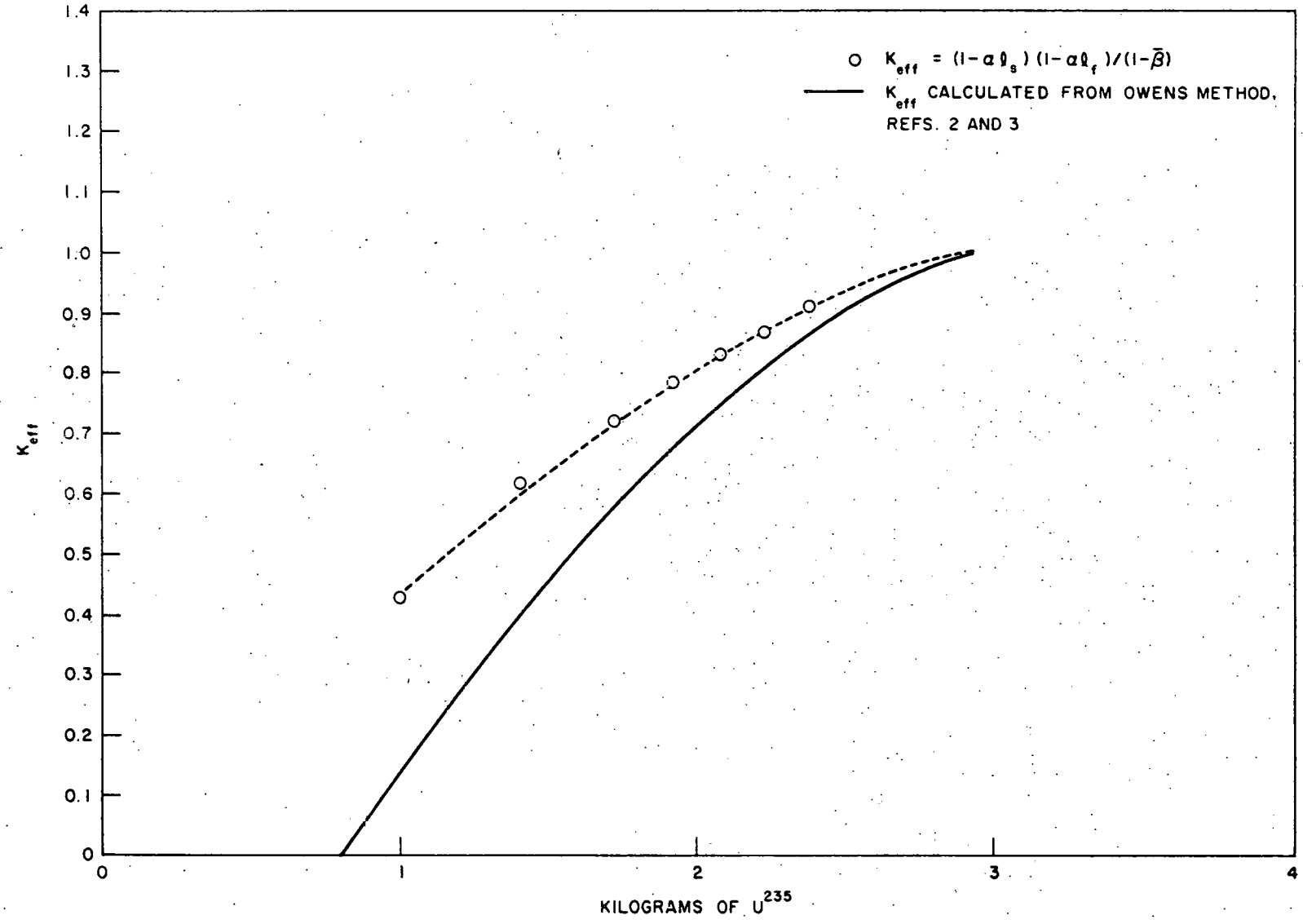

Fig. 20--K_{eff} versus kilograms of U^{235}

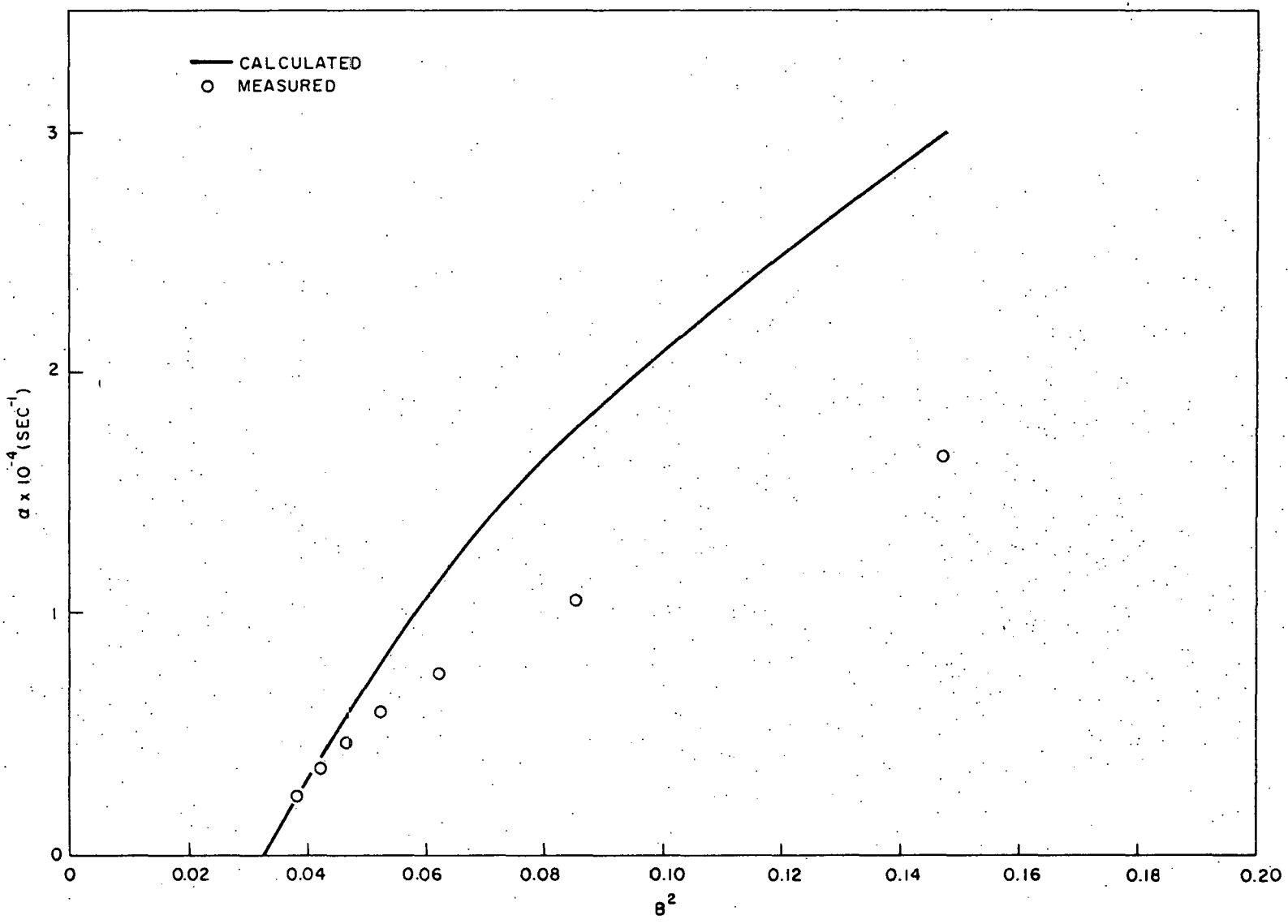

Fig. 21--α versus B^2 (extrapolation length = $0.71\bar{\lambda}_{tr}$)

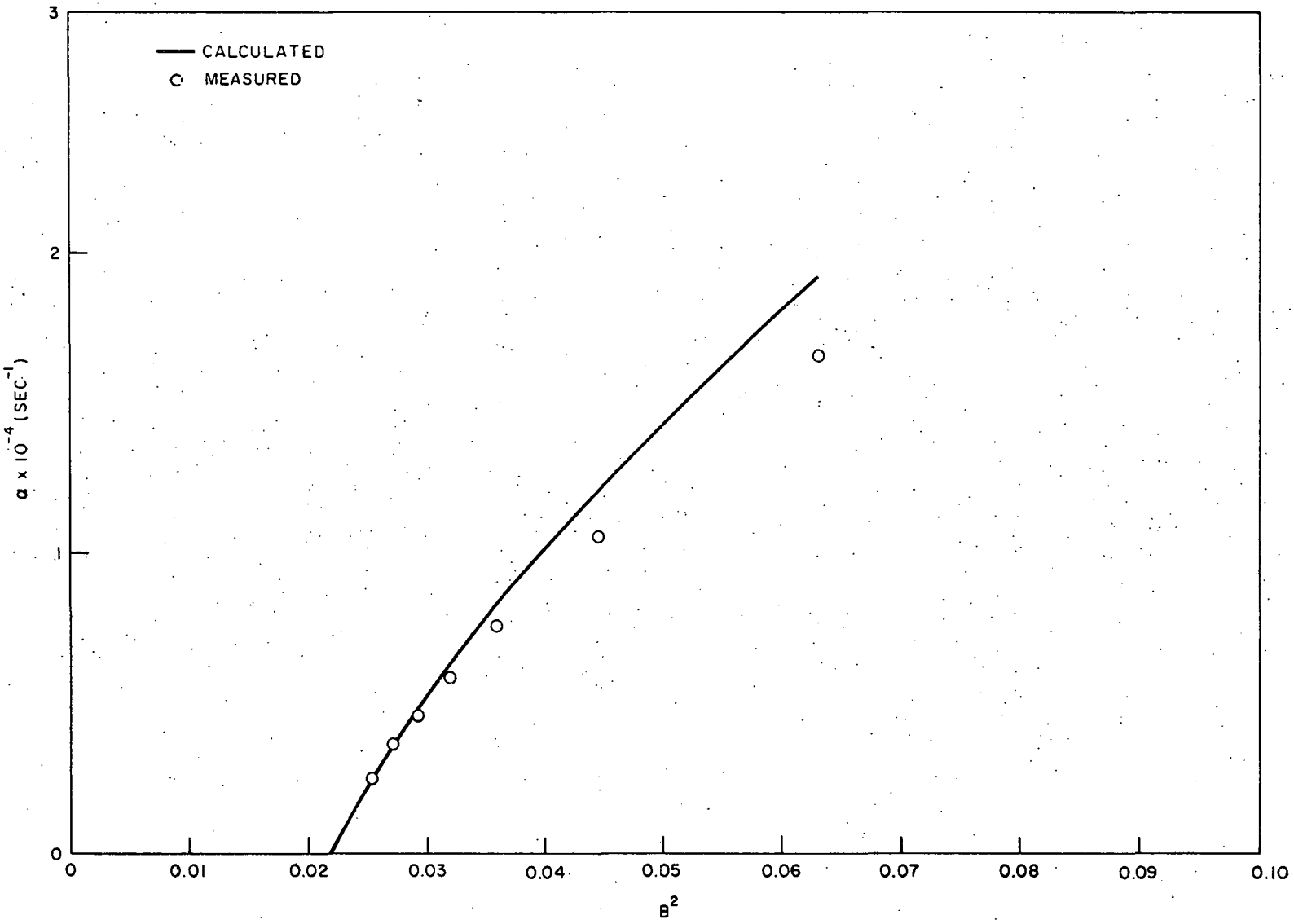

Fig. 22--α versus B^2 (extrapolation length determined from thermal flux plots)

from the electrons stopping in the lead produces neutrons with a near-fission spectrum from (γ, n) reactions. The experimental arrangement for the spectrum measurements is shown in Fig. 23. Both 16- and 50-m flight paths were used. The output of the BF_3 detectors was fed into a digital time module[9] developed at General Atomic. This time module was used in conjunction with a 256-channel analyzer to correlate the arrival time of the neutrons at the detector bank with a zero time associated with the initial neutron burst from the accelerator. From the known flight times and the known flight paths, the neutron energies were calculated.

To measure the scalar flux spectrum--which is the integral over all angles of the angularly dependent flux--in the assembly, a zirconium scatterer was placed in the glory hole to extract the neutron beam from the core. The method worked as follows: In order to measure the scalar flux spectrum in the assembly, the detector bank, through the collimating system, must view a scattering sample in the assembly that will integrate the angularly dependent flux without distorting it. It was found that a heavy incoherent scattering sample with a low absorption cross section would give these results. Investigations showed that zirconium placed in the glory hole permitted extraction of an undistorted scattered neutron spectrum. Comparisons of spectra measured by this method with those measured by previously tested methods gave good agreement. The use of this new technique eliminated the necessity of moving the subcritical assembly during the course of the high-neutron-flux measurements.

A scalar flux spectrum in pure water was measured in the core with the cadmium boundary defining the thickness of the tank as that calculated for the final loading. This spectrum is shown in Fig. 24. The theoretical curves shown were calculated using the free and bound hydrogen kernels for pure water. This measurement was made at 16 m. Figure 25 shows the scaler neutron spectrum in the multiplying assembly at 50 m and the spectrum in the core tank with boron–aluminum plates instead of uranium–aluminum plates at 16 m. The theoretical curves shown were calculated using the

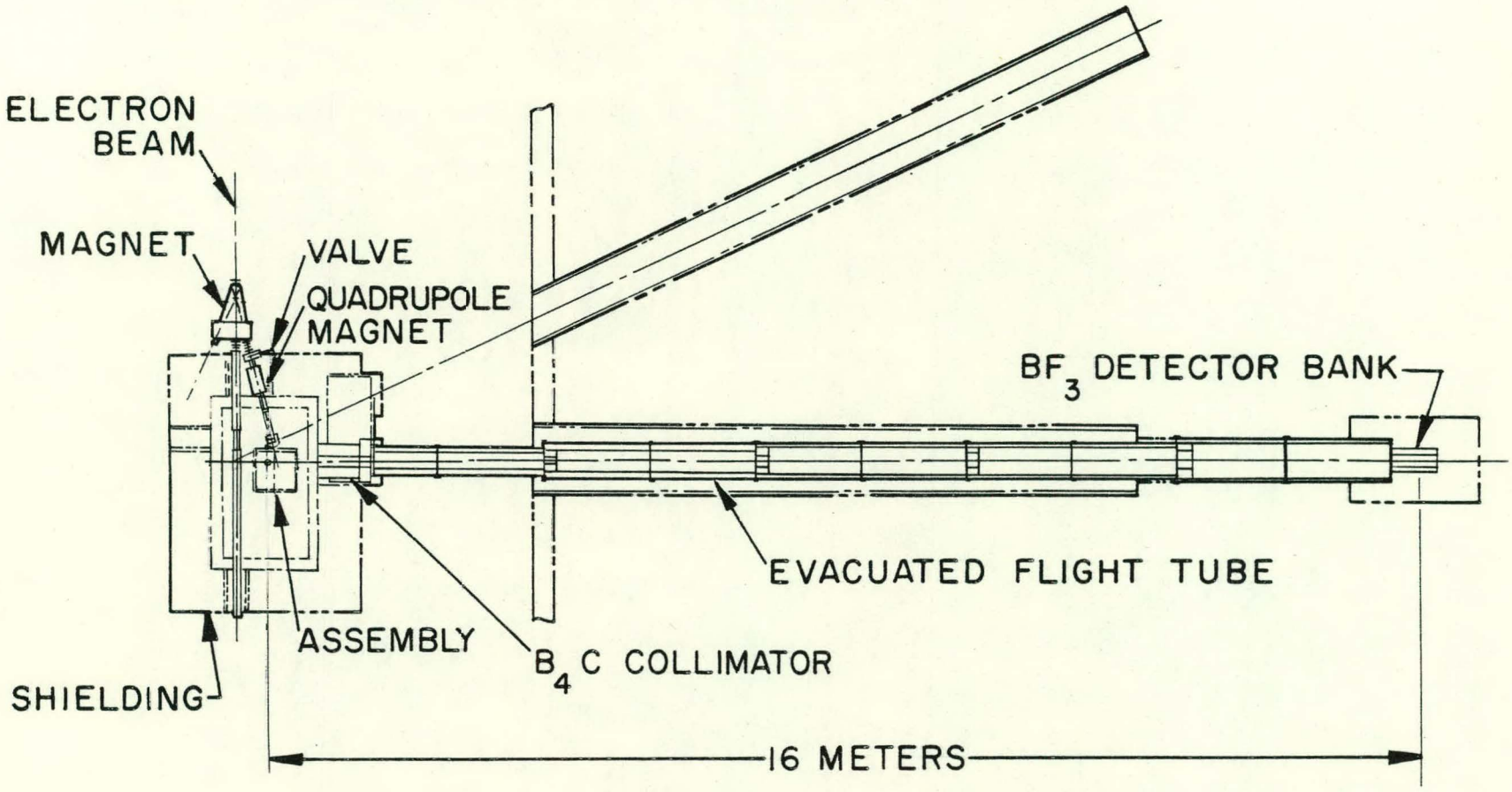

Fig. 23--Geometry for pulsed spectrum measurements

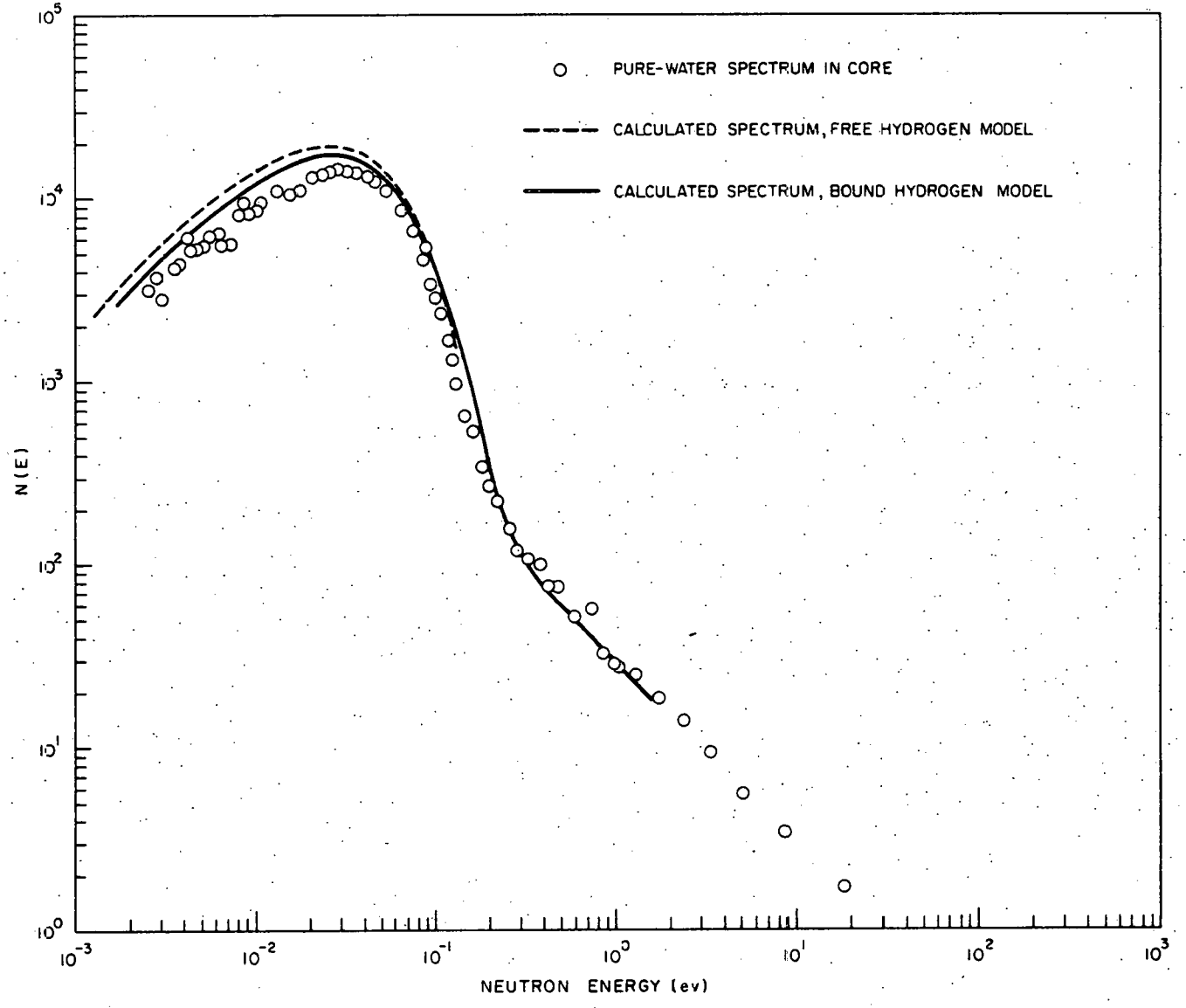

Fig. 24--Pure water spectrum measured in the subcritical tank

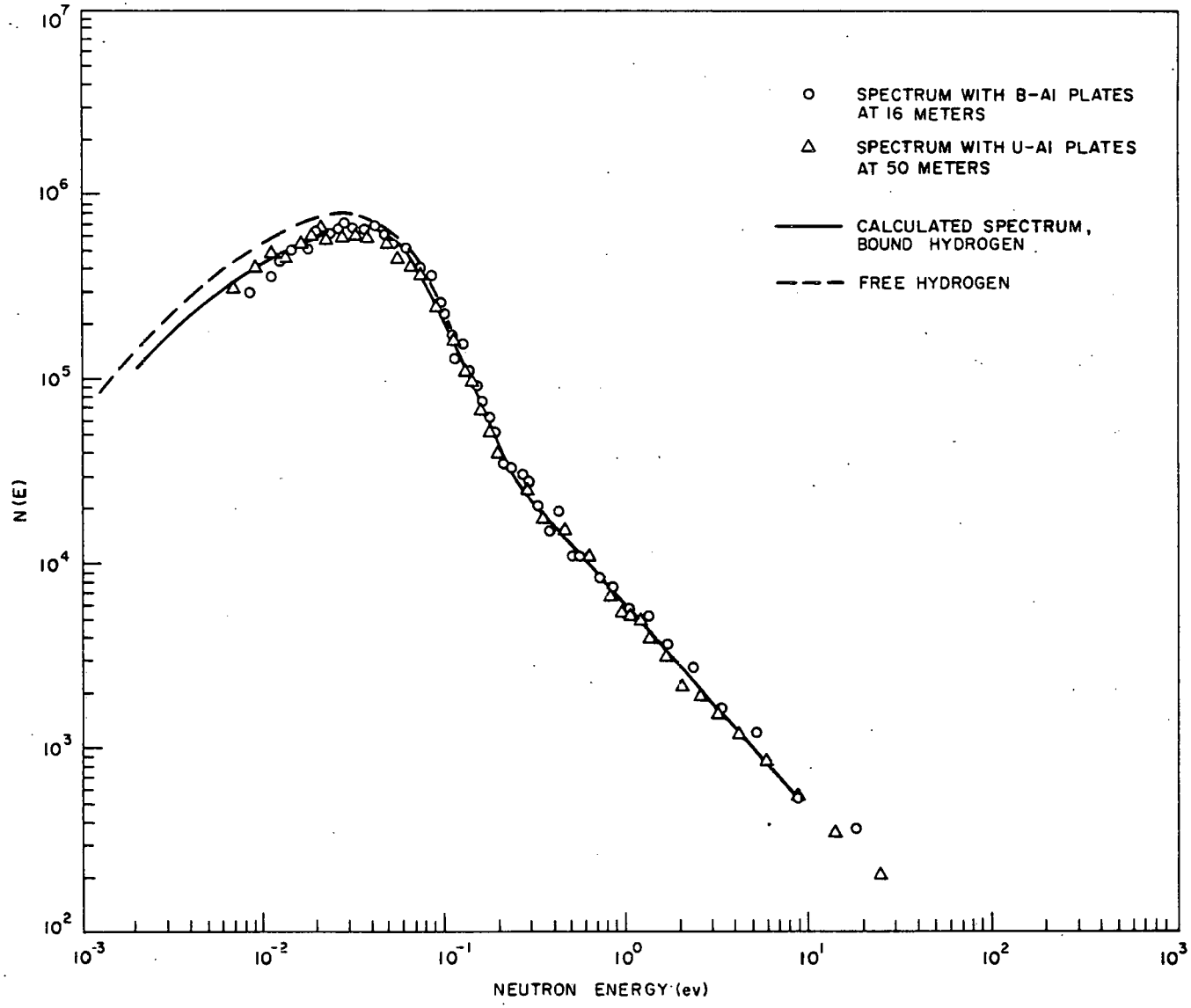

Fig. 25--Neutron spectra in multiplying and nonmultiplying assemblies

free and bound hydrogen kernels for homogeneously poisoned water.

5.4. FLUX MAPPINGS

Three flux mappings were taken in the subcritical assembly while the core was loaded with uranium–aluminum fuel plates to a thickness of 6.88 in. These flux mappings may be described as follows:

1. Axial flux mapping using cadmium-covered indium foils for measuring the epithermal (1.44 ev) flux. The indium foils were 0.25 in. in diameter and 0.002 in. thick. Each side of the foil was covered with cadmium 0.015 in. thick. The foils were positioned in a Plexiglas holder and inserted into the glory hole. The spacing between foils was approximately 1/4 in. This flux mapping is shown in Fig. 26.
2. Axial flux mapping using bare gold wires for measuring the thermal flux. These wires were a uniform 1/32 in. in diameter and were cut into lengths of 1/8 in. These wires were positioned in a Plexiglas holder which contained drilled holes just large enough to accommodate the wires. The wires were positioned so that the axis of the wire was perpendicular to the axial dimension of the assembly. The Plexiglas holder was inserted into the glory hole. These wires were also spaced 1/4 in. apart. This flux mapping is shown in Fig. 27.
3. Transverse flux mapping using bare gold wires for measuring the thermal flux. These wires were the same size as those used in the second type of flux mapping, described above. They were placed in a Plexiglas holder which had drilled holes just large enough to accommodate the gold wires. The spacing between wires was 1/2 in. The Plexiglas wire holder was inserted into a water channel between slots 12 and 13 of the assembly so that it was located 2.4 in. from the source side and 7 in. from one end of the assembly. This flux mapping is shown in Fig. 28.

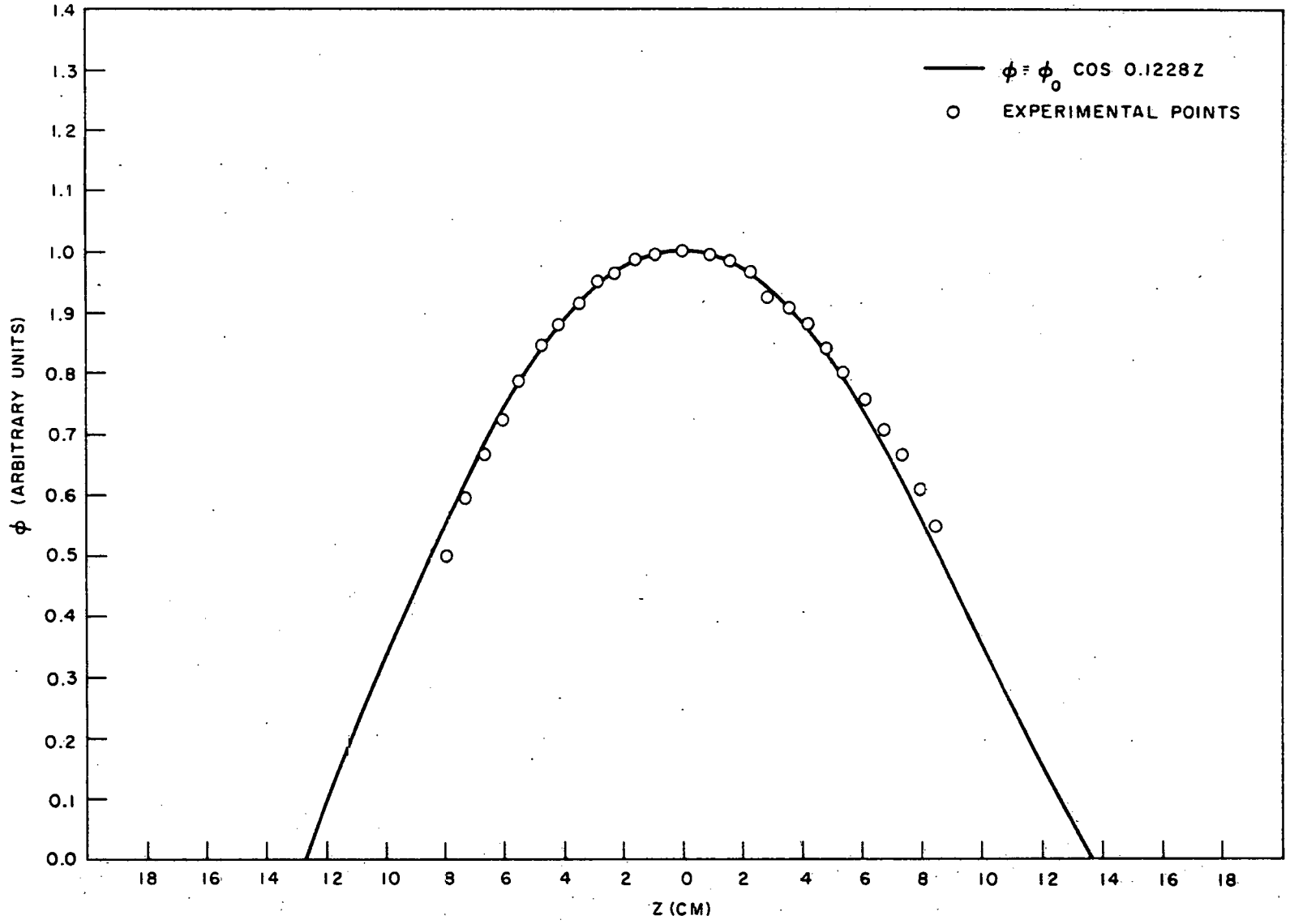

Fig. 26--Axial neutron flux using cadmium-covered indium foils at the last loading

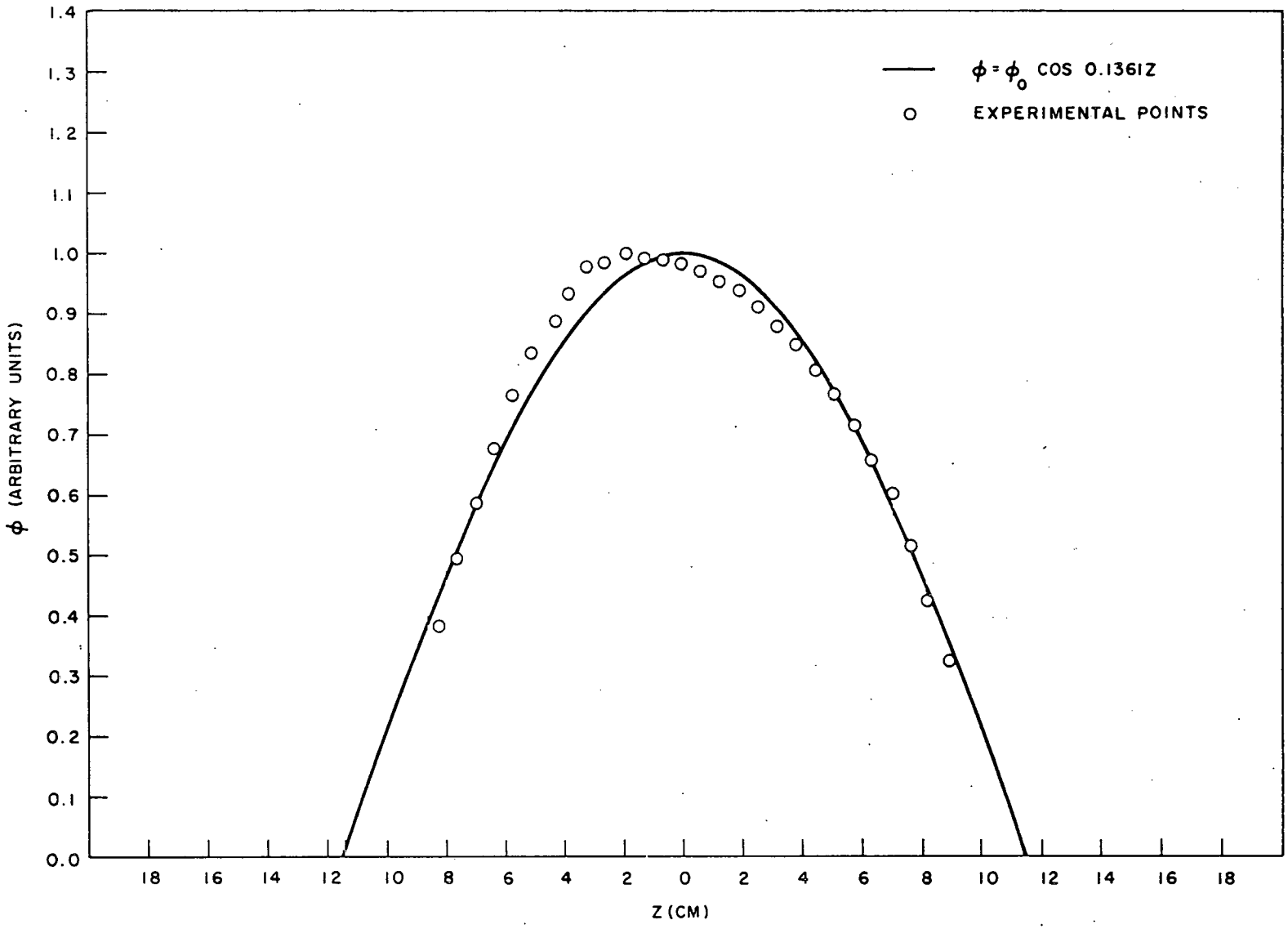

Fig. 27--Axial neutron flux using bare gold wires at the last loading

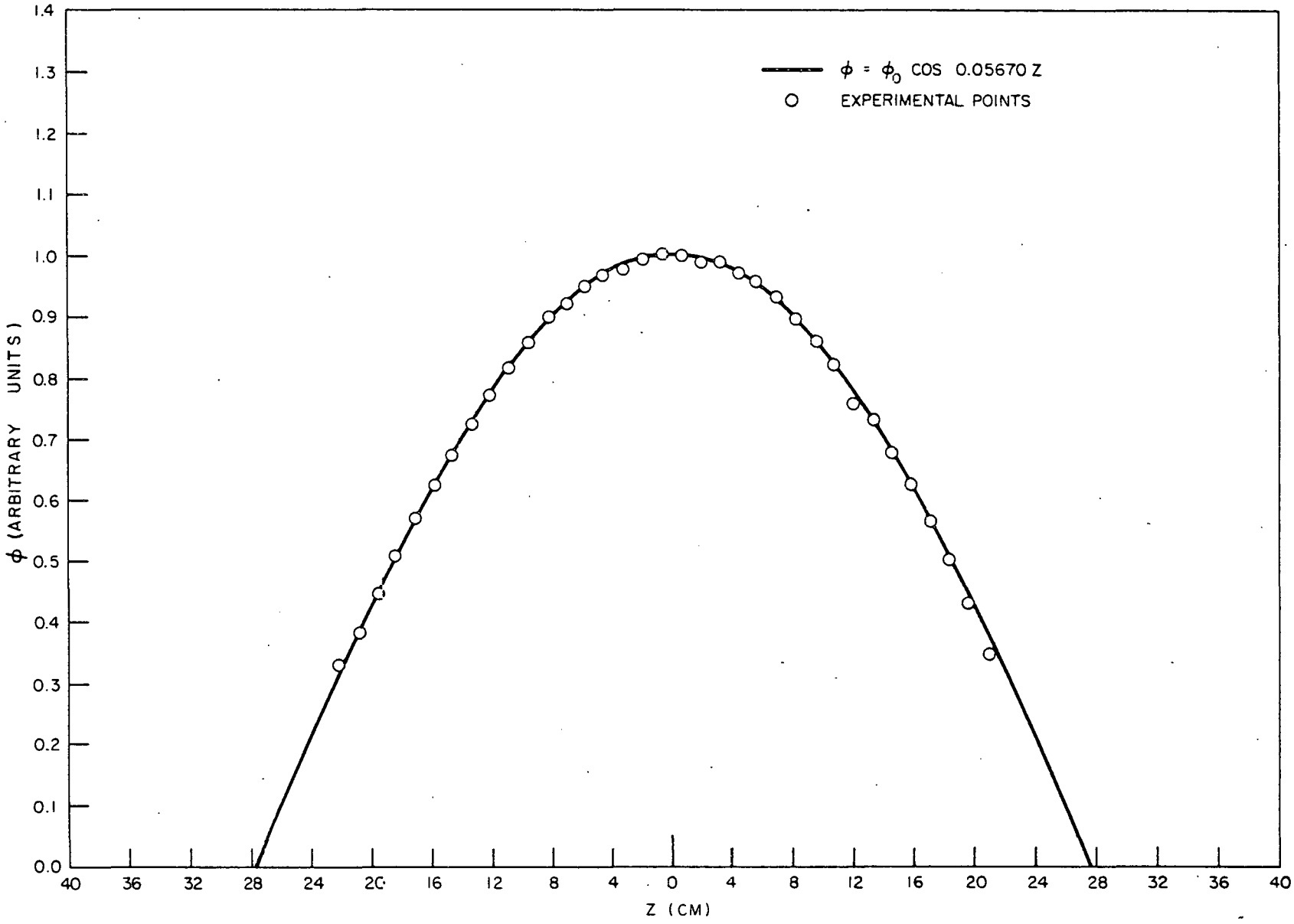

Fig. 28--Transverse neutron flux using bare gold wires at the last loading

The transverse and axial flux mappings were taken at the same time.

These three flux mappings were fitted by the ORPHEUS code to obtain the best extrapolation distance; this best fit is shown in Figs. 26, 27, and 28. The ORPHEUS code extrapolation distances are as follows:

Flux Mapping	Extrapolation Distance, ϵ (cm)
Axial, epithermal	3.9
Axial, thermal	2.65
Transverse, thermal	4.2

All three of the above flux mappings gave an experimental extrapolation distance ϵ larger than would be expected assuming the theoretical extrapolation distance of $\epsilon = 0.71\overline{\lambda}_{tr}$.

The transverse thermal flux demonstrated a nearly perfect cosine distribution, thereby denoting the expected absence of the higher even harmonics, since the source was located at the center of one face of the assembly.

Axial flux mapping were extended past the movable cadmium boundary and into the borated polyethylene which was used to back this boundary. The flux in the borated polyethylene followed the usual age-type solution. However, as would be expected, a large depression of the axial thermal flux occurred at this interface but appeared as a gray rather than a black region.

The integral counts obtained from a miniature fission counter employed in the time-dependence study of the die-away were used to obtain the axial thermal flux mapping shown in Fig. 29. The first 490 μsec of the integral count were discarded to ensure the absence of the higher harmonics. These data, when fitted to a cosine curve by the code ORPHEUS, gave an extrapolation distance of 2.9 cm. This value compares favorably with the value of 2.65 cm obtained from the axial thermal-flux mapping using gold wires.

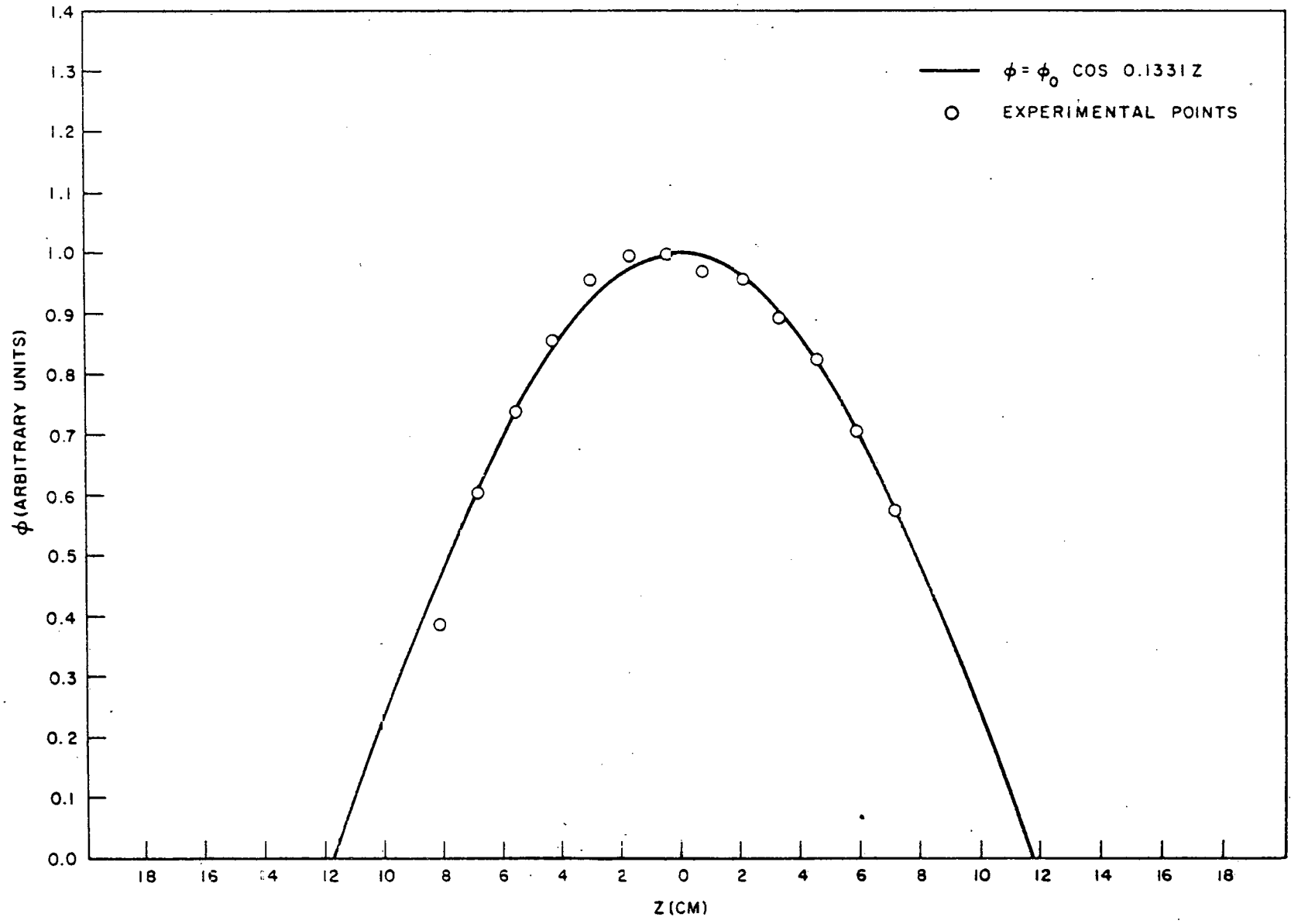

Fig. 29--Integral counts versus axial distance across core (490-μsec delay after the neutron pulse)

5.5. RADIATION LEVELS

Radiation levels around the subcritical assembly were monitored at two different positions. In each case the instrument used was a Nuclear Chicago Model-2586 QTπ-type instrument. One of the instruments was permanently affixed and monitored the radiation level 10.5 in. from the 6-in.-thick lead shield. This instrument was situated so as to measure the radiation level at the midpoint of the 18-in. by 18-in. face of the assembly through the lead shield after the assembly was shut down. The distance between the lead shielding and the 18-in. by 18-in. face of the assembly was 16 in. The unshielded radiation level was monitored with a portable QTπ at 3-1/2 in. from the midpoint of the 18-in. by 18-in. face of the assembly. Both the shielded and unshielded radiation levels of the subcritical assembly were measured without the light-water moderator being in the core.

Die-away measurements were made on every loading in the approach to a multiplication of 10. The operating conditions of the linear accelerator for these die-away measurements depended upon the multiplication of the core. The operating conditions of the accelerator for a multiplication of 10 are as follows:

Current	2 ma
Energy	19 Mev
Pulse rate	30 pps
Pulse width	0.5 μsec

The measured radiation level around the assembly after this particular die-away measurement was 19 mr/hr at the top of the assembly approximately 10 min after shutdown.

During the measurement of the neutron spectra, the accelerator was operated under the following conditions:

Condition	Length of Operation
Energy: 18 Mev Current: 60 ma Pulse rate: 30 pps Pulse width: 5 μsec	249 min
Energy: 18 Mev Current: 60 ma Pulse rate: 15 pps Pulse width: 5 μsec	420 min

The decay rate measured with a QTπ after the neutron-spectrum runs, at 3-1/2 in. from the midpoint of the 18-in. by 18-in. side of the subcritical assembly is given as follows:

Radiation Level (r/hr)	Time After Shutdown of Assembly (sec)
1.5×10^{1}	7.45×10^{2}
1.25×10^{1}	2.22×10^{3}
5.0×10^{-1}	1.06×10^{5}
5.3×10^{-2}	7.26×10^{5}
2.6×10^{-2}	9.60×10^{5}

The graph of the radiation level as a function of time appears in Fig. 9. The QTπ actually measured the radiation level of the source (a lead target) in addition to that of the core at early decay times; however, since this level was of the order of 300 mr/hr, it was neglected because it was less than the accuracy of the instrument. After about 30 min, the activity of the target had decayed to an insignificant level. At the later decay times, the QTπ measured the gamma-radiation level of the 5-curie PoBe source (approximately 2.5 mr/hr) and this value has been subtracted from the above values. The radiation level after the neutron-spectra run measured through the 6 in. of lead shielding by the permanently affixed QTπ was 21 mr/hr at 435 sec after shutdown of the assembly.

Housed in the neutron cave, the subcritical assembly had 6 in. of

lead shielding at the sides and on the bottom. It was necessary to shield the bottom because it was 4 ft off the floor. Since very little scattered radiation from the ceiling was expected in the cave, the top of the assembly was not shielded. When the radiation level at 3-1/2 in. from the core was 15 r/hr, the average radiation level in the neutron cave was about 25 mr/hr.

The fuel plates in the subcritical assembly contained an average of 17.14 g of U^{235} each. These plates were removed from the assembly and gamma and beta activity was measured approximately 271 hr after shutdown of the assembly. The gamma-radiation level measured at 12 in. from the midpoint of the fuel plate was 2.3 mr/hr and at 3 in. it was 9.5 mr/hr. The beta-plus-gamma radiation level measured at 12 in. from the midpoint of the fuel plate was 4.5 mrem/hr and at 3 in. it was 60 mrem/hr. These measured values were taken on the uranium–aluminum foil at the mid-position for the slot which is at the center of the assembly.

After operation of the assembly for the neutron-spectra measurements, a short-lived beta aerosol activity, which had a half life of approximately 30 min., was detected. This aerosol activity has been attributed to the daughters of noble gases which diffuse out of the fuel plates and into the atmosphere after the light-water moderator has been dumped from the core.[10] This aerosol activity was not very significant.

5.6. DETERMINATION OF THE URANIUM CONTENT IN THE FUEL PLATES

The method used for the determination of the amount of U^{235} in a fuel plate is based upon the density measurement of each of the uranium–aluminum fuel plates using Archimedes' principle. This method has been reported previously.[11]

Each fuel plate was cleaned, then weighed in air and in distilled water. The difference in these weights is therefore the volume of the fuel plate, and the density is simply the weight of the fuel plate in air divided by its volume. The weight-percent of total uranium in a fuel plate is then taken from a

curve of density versus weight-percent of uranium. For the purposes of the present investigation, the curve used was computed from the following equation after the substitution of the correct enrichment factor:[11]

$$X = \frac{(238.12 - 3.01f)(0.37037 - v)}{71.08 - 1.11f} \quad . \tag{32}$$

The appropriate value from this graph is multiplied by the total weight of the uranium–aluminum fuel plate and then by the enrichment of the uranium to obtain the grams of U^{235}. The procedure involved weighing each foil in air and water to the nearest 0.1 mg on a balance. The temperature of the distilled water bath was taken for each weighing and used as a correction for the density of the water bath. Since one-third of the foils had to have holes punched for the glory-hole re-entrant tube, 21 of these disks were used for chemistry analysis. The average difference between the density determinations and the chemistry analysis was 0.09 wt-%. Since the average weight of the fuel plates actually used in the subcritical assembly was 109.05 g, the average weight difference was about 0.09 g of U^{235}. The average weight of U^{235} per fuel plate was 17.14 g and therefore the density measurements were high by about 0.5%.

The density method for determining the U^{235} content of the uranium–aluminum fuel plates was also used by the supplier of the fuel plates, Sylcor. However, their method involved determining the U^{235} content for each core and using this average value and the weight of each fuel plate to determine the U^{235} content. Although the value of U^{235} per fuel plate obtained by these measurements varied from Sylcor's, the total U^{235} for all 250 fuel plates varied by only 0.6%, with our value being the larger. From these considerations, it seems fairly certain that the U^{235} content of the subcritical assembly was known within ±0.6%.

Several operations on the uranium–aluminum fuel plates were necessary before the actual loading into the core. Since the fuel plates were slip-fitted into supporting grooves, it was determined, using the borated-aluminum plates, that removing a 1/8-in. radius from each corner would greatly

facilitate loading and unloading the fuel plates. An average of 31 mg of uranium–aluminum alloy per fuel plate was lost by this operation. Re-entrant holes were punched in one-third of the fuel plates to accommodate a 9/16-in.-diameter glory hole. This was accomplished by means of a jig and punch. The punched disk was then saved to be reinserted at a later date or to be used for chemistry analysis. The dimple in the foil caused by the punching was about 0.002 in. maximum. The average weight of the punched pieces was 252 mg of uranium–aluminum alloy.

The uranium–aluminum fuel plates were coated with two coatings of crystal-clear Krylon and two coatings of a fluorocarbon spray. This plastic cladding was about 0.001 in. thick on each side of the fuel plate. The purpose of the cladding was to reduce the buildup of fission-product activity in the water. However, because the cladding was thin, the fission-product activity could possibly build up by fission-product recoil through the cladding. A sample of the core water was taken after the 669-min neutron-spectra measurement. The sample measured a gross beta activity of 3.5×10^{-5} $\mu c/cm^3$ 3.18 days after the assembly had been shut down.

Lucite spacers could not be inserted between the fuel plates near the safety-rod assembly. Therefore, these spacers were secured to the fuel plates by means of 0-80 screws threaded into the Lucite spacer, with the fuel plate being countersunk to accommodate the screw head. Spacers were placed on both sides of the fuel plates in one fuel-plate channel and none were placed on the fuel plates in the adjacent channels. To prevent the threads from stripping and allowing the spacers to fall off, the screws were dipped in a quick-drying epoxy resin before being secured to the fuel plate.

VI. SUMMARY OF RESULTS AND CONCLUSIONS

In summary, the purpose of the multiplying assembly was to create a clean geometry for unambiguous comparison of experimental data with theory. The boundary conditions outlined at the beginning of Section II were met satisfactorily, and the flexibility of the core will allow investigation of a wide variety of reactor configurations during future studies.

The empirical method discussed in Section IV appeared to be adequate to calculate the critical mass for the core. However, for K_{eff}'s much less than one, the disagreement between calculations based on the empirical method and experimental results became appreciable. The extrapolation of the inverse multiplication curves and the decay-constant curves seems to indicate the critical mass to be between 2.9 and 3.0 kg of U^{235}. This value agrees well with the calculated value of 2.9 kg of U^{235}. The disagreement between calculation and experiment for the mass of U^{235} for $K_{eff} = 0.9$ is less than 5%.

The calculated value of control-rod worth disagreed considerably with the values measured. The reason for this discrepancy is not known at present, but it may be caused by the method used to determine K_{eff} far from critical. Studies in this area should be attempted in the future.

The previous shielding calculations made for the core were incorrect by a factor of three owing to a lack of knowledge of actual operating conditions, but were in a conservative direction. When the calculations were redone for the actual conditions under which the core was operated, the calculated and theoretical shapes of the decay curves were the same and only the absolute power level of the core had to be adjusted. The equation for these calculations and a knowledge of the operating time of the core could then be used to predict the radiation expected in future experiments.

The primary objective of the experimental program under Project

Agreement No. 2 was to measure neutron spectra in the multiplying assembly in order to compare them with measurements in nonmultiplying assemblies poisoned to the same extent, and also with theory. Even though the measurements made during this program indicated a generally good agreement between the two measured spectra, more accurate measurements are necessary to study possible small differences. Prior to the use of the multiplying assembly, it was difficult to ensure that all spatial effects on measured spectra could be eliminated. Multiplication such as that obtainable with the core assembly described in this report is sufficient to reduce considerably the importance of spatial effects. The measurement of neutron spectra as a function of distance from control rods of various materials, sizes, and special cells will be simplified in the subcritical assembly. With a more nearly fundamental mode being employed, it is possible to distinguish more easily between changes due to the control rod or cell structure and those due to the spatial effects induced by the pulsed source.

The die-away measurements made in the core were very rewarding. By taking the assembly to a near-critical state and determining accurately the constants associated with the assembly, the K_{eff} for each loading could be determined accurately from Eq. (13), Section III. The buildup of thermal neutrons in the core predicted by the theory outlined in Section III was observed. Further experiments to determine more accurately the behavior of the higher harmonics would be desirable in the future. The results of such studies could be used to determine integral reactor parameters with a greater accuracy.

The extrapolation lengths observed from the flux mappings made in the core were somewhat larger than initially expected for thermal neutrons. However, over much of the core, this condition was probably caused by the fact that the thermal flux slaved to the fast flux. More thorough studies at different loadings are necessary to understand completely the results of these measurements. The possibility of the flux in the core being perturbed by foil spacing should also be studied. A parametric study of the buckling

versus the experimental decay constant in Eq. (14), Section III, would be further clarified by making axial flux measurements at all loadings in the core.

Appendix A

CROSS SECTIONS AND CONSTANTS ASSOCIATED WITH THE MULTIPLYING ASSEMBLY

Table 2 records the values of the parameters used to analyze the data from the multiplying assembly. They are not presented as "general constants" but only as the values which were used in the analysis of the subcritical assembly.

The cross sections listed as 2200 m/sec values in Column 3 of Table 2 are those from BNL-325. The parameters listed as average were obtained from

$$\overline{X} = \frac{\int_{0.002}^{0.2} X(E)\,\phi(E)\,dE}{\int_{0.002}^{0.2} \phi(E)\,dE} \tag{33}$$

where X is the particular parameter to be averaged and $\phi(E)$ is the scalar flux spectrum which was measured in the multiplying assembly at the last loading. These values were averaged using the computer code CRISS-CROSS.

The value of D is defined as

$$D(E) = \frac{1}{3\Sigma_{tr}(E)} = \frac{1}{3\left[\Sigma_s(E)(1 - \overline{\mu}) + \Sigma_a(E)\right]}. \tag{34}$$

$\Sigma_s(E)(1 - \overline{\mu})$ for hydrogen was calculated by the code ROBESPIERRE, which calculates the scattering kernel using Nelkin's bound model. $\Sigma_s(E)(1 - \overline{\mu})$ for oxygen was calculated similarly using a free-gas model. $\Sigma_s(E)$ for U^{235} and U^{238} was obtained from Refs. 12 and 13. $\Sigma_s(E)$ for aluminum was assumed to be constant and is the 2200 m/sec value from BNL-325. σ_a for U^{235} and U^{238} also was obtained from Refs. 12 and 13. The upper limit in Eq. (33) represents the energy at which the number of fissions

Table 2

SUBCRITICAL CONSTANTS

Parameter	Value	Comments
$N(H)$	$5.755(10)^{22}$	Atom densities in core (atoms/cm^3)
$N(U^{235})$	$1.676(10)^{20}$	
$N(U^{238})$	$1.200(10)^{19}$	
$N(O)$	$2.878(10)^{22}$	
$N(Al)$	$8.073(10)^{21}$	
H/U	343	Determined after final loading
$\sigma_a(U^{235})$	694 barns	2200 m/sec
$\sigma_a(U^{235})$	526.2 barns	Average
$\sigma_f(U^{235})$	582 barns	2200 m/sec
$\bar{\sigma}_f(U^{235})$	449.5 barns	Average
$\sigma_a(H)$	0.33 barn	2200 m/sec
$\bar{\sigma}_a(H)$	0.2616 barn	Average
$\sigma_a(Al)$	0.23 barn	2200 m/sec
$\bar{\sigma}_a(Al)$	0.182 barn	Average
$\sigma_a(U^{238})$	2.71 barns	2200 m/sec
$\bar{\sigma}_a(U^{238})$	2.186 barns	Average
Σ_a	0.129 cm^{-1}	2200 m/sec
$\bar{\Sigma}_a$	0.0996 cm^{-1}	Average
$\bar{D}$	0.179 cm	Average diffusion coefficient
L^2	1.80 cm^2	For analyzing the experimental data it was appropriate to use $L^2 = \bar{D}/\bar{\Sigma}_a$ and it is this value which is given
$\bar{E}$	0.06 ev	Average
$\bar{E}$ (epithermal)	1.3 ev	Energy averaged over the spectrum for $0.2 \leq E \leq 10$ ev
$\bar{v}$	$3.22(10)^5$ cm/sec^4	Average
β	0.0077	Effective fraction of delayed neutrons (Ref. 15)
η	2.07	2200 m/sec
$\bar{\eta}$	2.11	Average
ℓ_f	$6.2(10)^{-6}$ sec	Calculated using mean-emission-time technique with a black absorber to minimize upscattering
ν	2.47	Average number of neutrons produced per fission (see BNL-325)
B_o^2 (critical)	0.018 cm^{-2}	B_o^2 as determined using empirical method outlined in Section IV

becomes small. The total number of fissions for a given energy range was obtained from

$$\text{Total fission} = \int_{E}^{E'} \sigma_f(E)\, \phi(E)\, dE \ , \tag{35}$$

where the limits of integration are arbitrary and $\phi(E)$ is the measured scalar flux spectrum.

The calculation of the grams of U^{235} is covered in Section V. The atom densities used are based on the assumption that the material is homogenized over the entire core. The atom densities of U^{235} and hydrogen which were calculated prior to receiving the fuel elements differed by approximately 1% from the measured values. The calculation of ℓ_f, the fast lifetime, utilized the mean-emission-time technique as derived by Parks.[14] The technique is used to calculate the average time a neutron of energy E has spent in a moderating assembly before it leaves the assembly. This average time for neutrons of $E \leq 1$ ev was calculated using the infinite-medium diffusion theory code SPECTRUM. For the scattering kernels available, this code considers upscattering. Since the amount of upscattering above E = 0.1 ev is small, the calculation was made with a black absorber below 0.1 ev which prevented any upscattering from this black region. The slowing-down time[4] for the neutron from fission energy (about 2 Mev) to 1 ev was obtained from

$$t = \frac{\overline{\lambda}_s}{\xi} \sqrt{2m} \left(\frac{1}{\sqrt{E_1}} - \frac{1}{\sqrt{E_0}} \right) . \tag{36}$$

Table 3 is a record of some of the theoretical predictions and experimental results obtained with the multiplying assembly. The data are reported for each loading step in the approach to full multiplication whenever possible. Only the last value of the thickness was measured; the others are calculated values which assume a 0.145-in. unit cell. The 1/m values

Table 3

VALUES OBTAINED AT EACH LOADING

	LOADING								
	1	2	3	4	5	6	7	8	9
Core width, in.	1.57	3.02	4.18	4.50	5.06	5.64	6.07	6.50	6.88
U^{235}, g/load	513.68	489.13	411.46	154.19	154.08	205.51	154.21	154.14	154.15
U^{235}, total g	513.68	1002.81	1414.27	1568.46	1722.54	1928.05	2082.26	2236.40	2390.55
H_2O, g/load	7300	6637	5309	1991	1991	2655	1991	1991	1719
H_2O, total g	7300	13937	19246	21238	23229	25883	27874	29865	31584
Al, g/load	2710.42	2767.50	2173.60	815.34	813.40	1085.36	817.57	816.88	811.72
Al, total g	2710.42	5477.92	7651.52	8466.86	9280.26	10365.62	11183.19	12000.07	12811.79
B^2 (calc), cm^{-2}	0.260	0.078	0.046	0.041	0.034	0.030	0.026	0.024	0.022
B^2 (exper), cm^{-2}		0.063	0.044		0.036	0.032	0.029	0.027	0.025
B^2 $(0.7104\bar{\lambda}_{tr})$, cm^{-2}	0.446	0.148	0.085	0.076	0.062	0.052	0.047	0.042	0.038
$\ell_s \times 10^{-6}$ (exper)		31.31	32.40		32.92	33.19	33.35	33.49	33.6
$\ell_s \times 10^{-6}$ (calc)		30.48	32.31		33.04	33.34	33.55	33.69	33.83
α_- (calc), sec^{-1}		2.73×10^4	1.72×10^4		1.15×10^4	0.861×10^4	0.679×10^4	0.491×10^4	0.346×10^4
α_- (exper), sec^{-1}		1.65×10^4	1.05×10^4		0.748×10^4	0.578×10^4	0.459×10^4	0.360×10^4	0.244×10^4
α_+ (calc), sec^{-1}		16.7×10^4	17.5×10^4		18.0×10^4	18.3×10^4	18.4×10^4	18.6×10^4	18.7×10^4
α_+ (exper), sec^{-1}		17.4×10^4	18.0×10^4		18.3×10^4	18.5×10^4	18.6×10^4	18.7×10^4	18.8×10^4
K_{eff} (calc)	0.01	0.140	0.400	0.464	0.580	0.680	0.745	0.816	0.870
K_{eff} (exper)		0.44	0.62		0.72	0.78	0.83	0.87	0.91
1/m (ion chamber 1)		0.62	0.44	0.40	0.35	0.28	0.25	0.21	0.17
1/m (ion chamber 2)		0.70	0.43	0.39	0.33	0.26	0.23	0.19	0.14
1/m (fission counter)		0.94	0.64	0.60	0.56	0.50	0.42	0.36	0.29
Rod worth (calc), ΔK									0.066
Rod worth (exper), ΔK									0.02

normalized to the first loading were determined from

$$\left(\frac{1}{m}\right)_n = \left(\frac{1}{m}\right)_{n-1} \frac{C_{n-1}}{C_n} \quad , \tag{37}$$

where C_{n-1} and C_n were counts taken on the same day and n denotes the loading.

The K_{eff}'s, geometric bucklings, and rod worths designated as calculated were determined prior to loading the core, using the empirical method outlined in Section IV. The K_{eff}'s listed as experimental were determined from Eq. (13), Section III, and the values from Table 2. ℓ_s(exper) was used and is defined as

$$\ell_s(\text{exper}) = \frac{1}{\Sigma_a v + \bar{D} B^2(\text{exper})} \quad .$$

B^2(exper) was calculated using the measured extrapolation distance at the last loading. ℓ_s(calc) was determined using B^2(calc) instead of B^2(exper).

α_-(exper) is the measured decay constant. The α_+(exper) was calculated using Eq. (14), Section III, and the K_{eff}(exper). $\alpha\pm$ (calc) was determined using Eq. (14), Section III, and the K_{eff}(calc).

The rod worth (exper) was determined from measured decay constants and Eq. (13), Section III.

Appendix B

SHIELDING CALCULATIONS

The following assumptions will be made in computing the radiation level of the subcritical assembly because they follow very closely the actual circumstances under which the measurements were made:

1. The radiation level will be determined at 9 cm from the 18-in. by 18-in. face of the subcritical assembly at the midpoint of the face.
2. When the radiation level is measured, only uranium–aluminum fuel plates will be in the core; i. e., no water will be in the core.
3. The decay rate used will be for the total gamma-ray energy following assembly shutdown after operation for 10 hr.

The exposure rate at a distance R cm from a point gamma source of C curies in air, within ±10%, is

$$\text{Dose rate at distance R cm from C-curie source} = 5.2 \times 10^{6} \frac{CE}{R^{2}} \text{ mr/hr} .$$

If an absorbing material of thickness t cm and (total) absorption coefficient μ cm^{-1} is placed between the source and the point at which the dose is being calculated, then the above expression becomes

$$\text{Dose rate at distance R cm from C-curie source with t-cm absorber} = 5.2 \times 10^{6} \frac{CE\, e^{-\mu t}}{R^{2}} \text{ mr/hr} .$$

Consider the case of an isotropic circular plane (disk) source of radius a, with the detector on the normal passing through the center. Let the source strength S be the total number of curies per square centimeter. Consider in the source a narrow annulus of radius x and width dx and everywhere a distance R from the detector. The dose rate at R from the annulus is $(5.2 \times 10^{6}\ E\ 2\pi x dx S)/(R^{2})$, where C has been replaced by $2\pi x dx S$.

The corresponding value for the whole disk source is then obtained by integrating over-all values of x from zero to a; the result is given by

$$I = (5.2 \times 10^6 E)(2\pi S) \int_o^a \frac{x\,dx}{R^2} . \qquad (38)$$

Since $R^2 = x^2 + z^2$, where z is the perpendicular distance from the plane source to the detector, it follows that $RdR = xdx$ and, hence,

$$I = (5.2 \times 10^6 E)(2\pi S) \int_z^{\sqrt{z^2+a^2}} \frac{dR}{R} . \qquad (39)$$

Integration of the above expression gives

$$I = 5.2 \times 10^6\, \pi SE \left[\ln \left(\frac{a^2 + z^2}{z^2} \right) \right] . \qquad (40)$$

In order to include self-absorption, it is assumed that the subcritical assembly is divided into n equal slabs of thickness t. In the above expression, z is the fixed distance to the face of the first slab and, in general, the distance to the face of the n^{th} slab is $z + (n - 1)t$. Therefore, the dose rate from the n^{th} slab, including self-absorption, may be written as

$$Ip(n) = 5.2 \times 10^6 \pi SE \left\{ hr \left[\frac{a^2}{(z + (n - 1)t)^2} \right] \right\} e^{-(n-1)\mu t} , \qquad (41)$$

where μ (in cm^{-1}) is the average linear absorption coefficient for the reactor.

The total dose rate as seen by the detector is obtained by summation of the dose rates from all n slabs, or

$$Ip(total) = \sum_1^n Ip(n) . \qquad (42)$$

The source strength (Mev/watt-sec) at any time after shutdown of the reactor may be obtained from graphs, such as those presented in Ref. 6.

These graphs are for various operating times, i.e., 1, 10, 100, and 1000 hr.

If the delayed gamma radiation in the core, at some time t after reactor shutdown, is Y Mev/watt-sec, then the curie strength of the core is

$$C = \frac{(Y)(W)}{(E)(3.7 \times 10^{10})} , \tag{43}$$

where E is the average gamma-ray energy per disintegration and W is the average power level at which the core has been operating. To obtain S, Eq. (43) must be divided by the total surface area of the core. The total surface area is just the actual surface area of one slab times the number n of imaginary slabs into which the core has been divided, or $n\pi a^2$, where πa^2 has been taken to equal in area the actual area of the square face of the subcritical assembly. Dividing C by this area and inserting the result into Eq. (41) for S gives

$$Ip(n) = \frac{(1.4 \times 10^{-4})(Y)(W)}{na^2} \left\{ 1\mu \left[\frac{a^2}{(z + (n-1)t)^2} + 1 \right] \right\} e^{-(n-1)\mu t} , \tag{44}$$

showing that Ip(n) is independent of the assumed average gamma-ray energy per disintegration.

The average linear absorption coefficient for the reactor, μ, was obtained by dividing the weight of all material in the reactor by the total volume of the core to get an average density and then multiplying this average density by the average mass absorption coefficient. Only the fuel plates were in the core when the radiation levels were observed, since the water moderator had to be dumped before entry into the shielded neutron cave. Since the fuel plates are 84 wt-% aluminum and 16 wt-% uranium, the mass absorption coefficient was weighted accordingly.

In the derivation of the above equations, it was assumed that the square face of the subcritical assembly could be replaced by a circle. If the radius, a, of the circle is 25.8 cm, then the circle has an area

equivalent to the area of the 18-in. by 18-in. face of the subcritical assembly. The radiation level of the assembly was measured at 9 cm from the mid-point of the 18-in. by 18-in. face and is denoted by z in Eq. (44). The values of n and t have been arbitrarily chosen as 17 and 1.0 cm, respectively. When these values of n from 1 to 17 are carried out according to Eq. (42), the dose rate from the entire assembly may be reduced to the simplifed expression,

$$Ip(total) = 2.2 \times 10^{-10} \; Y \; W \; r/hr \; . \qquad (45)$$

This result is then a product of four factors, two of which are the self-absorption and the geometry; the third is the average power level (W) of the core; and the fourth is the normalized decay rate (Y) for the total gamma-ray energy. If self-absorption were entirely neglected, the total radiation level Ip(total) would be increased by 20%. In Eq. (45) the least known factor is the average power level, estimated to be 3 watts. If this value is assumed, then Eq. (45) becomes

$$Ip(total) = 6.6 \times 10^{-10} \; Y \; r/hr \; . \qquad (46)$$

REFERENCES

1. Beyster, J. R., J. L. Wood, W. M. Lopez, and R. B. Walton, "Measurements of Neutron Spectra in Water, Polyethylene, and Zirconium Hydride," Nuclear Sci. and Eng., Vol. 9, 1961, p. 168.

2. Owen, B. G., and R. A. Gibson, "An Empirical Correlation of the Experimental Data on Homogeneous, Highly Enriched Uranium–Hydrogen Critical Assemblies--I. Changes in Geometry," J. Nuclear Energy, Part B, Reactor Technology, Vol. 1 1959, p. 10.

3. Ibid., "II. Changes in Physical Properties," J. Nuclear Energy, Part B, Reactor Technology, Vol. 1, 1959, p. 92.

4. Glasstone, S., and M. C. Edlund, The Elements of Nuclear Reactor Theory, D. Van Nostrand and Company, New York, 1952.

5. Schultz, M. A., Control of Nuclear Reactors and Power Plants, McGraw-Hill Book Company, Inc., New York, 1955.

6. Perkins, J. F., and R. W. King, "Energy Release from the Decay of Fission Products," Nuclear Sci. and Eng., Vol. 3, 1958, p. 726.

7. Young, J. C., J. R. Beyster, P. R. Heid, D. H. Houston, and G. D. Trimble, Development of Multiplying Assembly, First Quarterly Report, General Atomic, Report GA-1813, November 14, 1960.

8. Ibid., Second Quarterly Report, General Atomic, Report GA-1957, January 20, 1961.

9. Nather, R. E., "An All-transistor Time Analyzer Attachment for Multi-channel Pulse Height Analyzers," Trans. Am. Nuclear Soc., Vol. 3, No. 1, 1960, p. 286.

10. Bolton, P. R., et al., "Aerosol Activity from Experimental Low-power Reactor Operation," Health Physics, Vol. 1, No. 2, 1958, p. 135.

11. Aronin, L. R., and J. K. Klein, Use of a Density (Specific Volume) Method as a Sensitive Absolute Measure of Alloy Composition, and Its Application to the Aluminum–Uranium System, Nuclear Metals, Inc., Report NMI-1118, October, 1954.

12. Wikner, N. F., and S. Jaye, Energy-dependent and Spectrum-averaged Thermal Cross Sections for the Heavy Elements and Fission Products for Various Temperatures and C:U^{235} Atom Ratios, General Atomic, Report GA-2113, June 16, 1961.

13. Goodjohn, A. J., and N. F. Wikner, Suggested Values for the Partial Cross Sections of U^{235} for Use in the Neutronic Analysis of Thermal and Intermediate Reactors, General Atomic, Report GA-2151, July 17, 1961.

14. Unpublished data.

15. Carroll, E. E., Jr., N. Hartmann, and D. Klein, Pulse Neutron Measurements and Subcritical Lattices, Westinghouse Atomic Power Division, Report WAPD-R(D)-7, April, 1961.